

13. SITE 937¹

Shipboard Scientific Party²

HOLE 937A

Date occupied: 27 April 1994
Date departed: 27 April 1994
Time on hole: 5 hr, 30 min
Position: 4°35.731'N, 47°12.432'W
Bottom felt (drill pipe measurement from rig floor, m): 2771.3
Distance between rig floor and sea level (m): 11.14
Water depth (drill pipe measurement from sea level, m): 2760.2
Penetration (m): 0.20
Number of cores (including cores having no recovery): 1
Total length of cored section (m): 0.20
Total core recovered (m): 0.21
Core recovery (%): 100
Oldest sediment cored:
Depth (mbsf): 0.20
Nature: Silty clay
Earliest age: Pleistocene

HOLE 937B

Date occupied: 27 April 1994
Date departed: 28 April 1994
Time on hole: 18 hr, 45 min
Position: 4°35.749'N, 47°12.449'W
Bottom felt (drill pipe measurement from rig floor, m): 2771.0
Distance between rig floor and sea level (m): 11.14
Water depth (drill pipe measurement from sea level, m): 2759.9
Penetration (m): 180.30
Number of cores (including cores having no recovery): 19
Total length of cored section (m): 180.30
Total core recovered (m): 159.71
Core recovery (%): 88
Oldest sediment cored:
Depth (mbsf): 180.30
Nature: Silty clay
Earliest age: Pleistocene

HOLE 937C

Date occupied: 28 April 1994
Date departed: 28 April 1994
Time on hole: 7 hr, 45 min
Position: 4°35.760'N, 47°12.444'W
Bottom felt (drill pipe measurement from rig floor, m): 2767.5
Distance between rig floor and sea level (m): 11.17
Water depth (drill pipe measurement from sea level, m): 2756.3
Penetration (m): 76.50
Number of cores (including cores having no recovery): 9
Total length of cored section (m): 76.50
Total core recovered (m): 80.52
Core recovery (%): 105
Oldest sediment cored:
Depth (mbsf): 76.50
Nature: Silty clay
Earliest age: Pleistocene

HOLE 937D

Date occupied: 28 April 1994
Date departed: 28 April 1994
Time on hole: 1 hr, 30 min
Position: 4°35.773'N, 47°12.444'W
Bottom felt (drill pipe measurement from rig floor, m): 2768.3
Distance between rig floor and sea level (m): 11.17
Water depth (drill pipe measurement from sea level, m): 2757.1
Penetration (m): 16.70
Number of cores (including cores having no recovery): 2
Total length of cored section (m): 16.70
Total core recovered (m): 17.26
Core recovery (%): 103
Oldest sediment cored:
Depth (mbsf): 16.70
Nature: Silty clay
Earliest age: Pleistocene

Principal results: Site 937 (proposed Site AF-17) is located on the eastern part of the Amazon Fan, on the crest of the western levee of the abandoned Yellow Channel-levee System. The site was intended to provide a hemipelagic biostratigraphic and magnetostratigraphic reference section above the Yellow Channel-levee System and to sample the upper part of the levee crest for comparison with Site 933.

¹Flood, R.D., Piper, D.J.W., Klaus, A., et al., 1995. *Proc. ODP, Init. Repts.*, 155: College Station, TX (Ocean Drilling Program).

²Shipboard Scientific Party is as given in the list of participants in the contents.

The site was originally selected on the eastern levee crest (*Farnella* seismic-reflection profile, FR815; 0758 hr on 12 Jan.). Because the 3.5-kHz profile obtained during the pre-site survey from *JOIDES Resolution* showed that sediment on the eastern levee was more slumped than expected, we relocated the site 2 km to the west, on the western levee crest.

Hole 937A was cored by APC to 0.2 mbsf. A longer mud-line core was obtained at Hole 937B, which was cored by APC to 83.5 mbsf, then by XCB to 180.3 mbsf, with total hole recovery of 159.71 m (88.6%). Hole 937C was cored to 76.5 mbsf and recovered 80.52 m (105.2%). The pressure core sampler (PCS) was used from 75.5 to 76.5 mbsf, but recovered no sample. Hole 937D was cored to 16.7 mbsf and recovered 17.26 m (103.3%).

Temperature measurements were made at 54 and 84 mbsf (ADARA) in Hole 937B, showing a mean geothermal gradient of 31°C/km. There was gas expansion in many cores, most severely at about 60 mbsf. Methane was found throughout the hole, but higher hydrocarbons were not detected.

Two lithologic units are recognized:

Unit I (0–0.85 mbsf) is a Holocene bioturbated, nanofossil-foraminifer clay, containing 48% carbonate at the mud line, decreasing to 8% at 0.5 mbsf. The unit includes four indurated iron-rich clay crusts between 0.15 and 0.38 mbsf.

Unit II (0.85–180.30 mbsf) consists of mud with interbedded laminae and beds of silt and very fine sand. The unit is subdivided into four subunits. Subunit IIA (0.85–10.50 mbsf) comprises mud that it is intensely bioturbated. At the base of the subunit is a 2.3-m-thick mud with particularly intense black coloration from hydrotroilite (>1% total sulfur) with steeply dipping boundaries, possibly corresponding to diagenetic activity along a fault. Subunit IIB (10.49–37.43 mbsf) comprises mud, with only indistinct mottling. Rare pale-blue vivianite patches are present. This subunit is probably the lateral equivalent of the Blue Channel-levee System, 10 km distant at Site 938. Subunit IIC (37.43–93.51 mbsf), corresponding to the top of the Yellow levee crest, consists of faintly mottled mud with a few laminae and thin beds of silt. The frequency and thickness of silt laminae and beds vary on a scale of a few meters. Large burrows, 1–2 cm in diameter, concentrated along the tops of silt beds were probably formed by echinoids, whose spines are a common component of the sediment. Subunit IID (93.51–180.3 mbsf) consists of faintly mottled mud with laminae and thin beds of silt and fine sand. Sand beds are as thick as 10 cm and some are cross-laminated. Below 153 mbsf, sediment appears disturbed and includes several carbonate-rich intervals. This subunit also appears to be part of the Yellow levee.

Calcareous nanofossils are rare or absent in Unit II. Foraminifer abundances are generally moderate in Subunits IIA and IIB and are low in Subunits IIC and IID. Aragonitic pteropods are found throughout Unit II. Wood fragments are abundant in the lower part of Subunit IID. Unit II can be constrained in age to less than 40 ka by the absence of *P. obliquiloculata*.

No magnetic excursion was detected at this site. Variation in magnetic declination, interpreted as secular variation, is well-developed between 1 and 45 mbsf, corresponding to the interval of the Amazon, Aqua, Purple, and Blue Channel-levee systems. Thirty-four cycles were detected, with wavelength increasing downhole. At Sites 931 and 933, the Lake Mungo magnetic excursion (30 ka) was detected just below the Blue seismostratigraphic interval, so the age of the 1- to 45-mbsf interval is inferred to be 10 to 25–28 ka. This implies that the cycles are of average 500-yr duration, similar to those inferred from archeological and observatory data.

Total organic carbon content is almost constant at 1% from 20 mbsf to the base of the hole. Total sulfur exceeds 0.5% between 3.5 and 11 mbsf.

This site will provide a long reference isotopic and magnetostratigraphic section in bioturbated muds corresponding to the Amazon, Aqua, Purple, and Blue Channel-levee systems. The site also sampled part of the Yellow levee. The total thickness of the levee is unclear from seismic reflection data, but could be as great as 450 m. As noted at other sites, there is considerable variation in the abundance of silt and sand beds in the levee sections. Asymmetric cycles in the frequency of these beds are not apparent; rather, the beds tend to occur in clusters or packets. This may indicate a source influence on turbidite sedimentation that is perhaps related to climatic or sea-level fluctuations or autocyclic changes in river-mouth sedimentation. The correlative section of the Yellow levee in Site 933 on the middle fan also shows fluctuations in the abundance of silt laminae.

SETTING AND OBJECTIVES

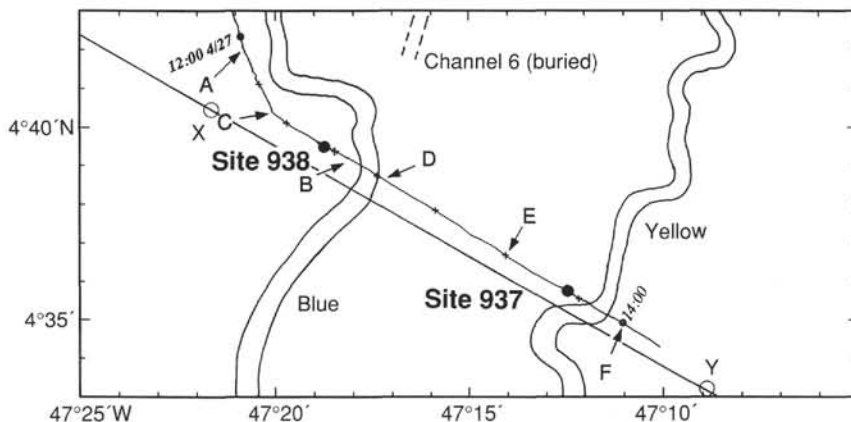
Introduction

Site 937 (proposed Site AF-17), located on the eastern portion of the Amazon Fan, was intended to provide a hemipelagic reference section in relatively shallow water (2760 m) above the crest of the Yellow System and to sample the upper part of the Yellow levee crest. The Yellow System was sampled at Site 933 in deeper water, and this hole provided the opportunity to sample the same system in shallower water.

Setting

Site 937 is located on the eastern part of the Amazon Fan, on the crest of the western (left) levee of the Yellow System near the shallowest depth to which it can be traced as a bathymetric feature (Fig. 1; Damuth et al., 1988; Manley and Flood, 1988). Cores recovered at Site 933 suggested that the Yellow System is younger than 30 ka (post-dating the Lake Mungo magnetic excursion), and thus we expected to recover a biostratigraphic record almost 30,000 years long at this site. This site, Site 938 (proposed Site AF-16), and Site 939 (proposed Site AF-12) are the shallowest-water sites to be drilled during Leg 155.

Figure 1. Location of Sites 937 and 938 showing the *JOIDES Resolution* ship track. X–Y is the seismic profile shown in Figure 2. E–F is the 3.5-kHz profile shown in Figure 3. A–B and C–D are profiles illustrated in Figures 1 and 2 of the “Site 938” chapter, this volume. Channel locations are based on GLORIA sidescan images (Damuth et al., 1988).



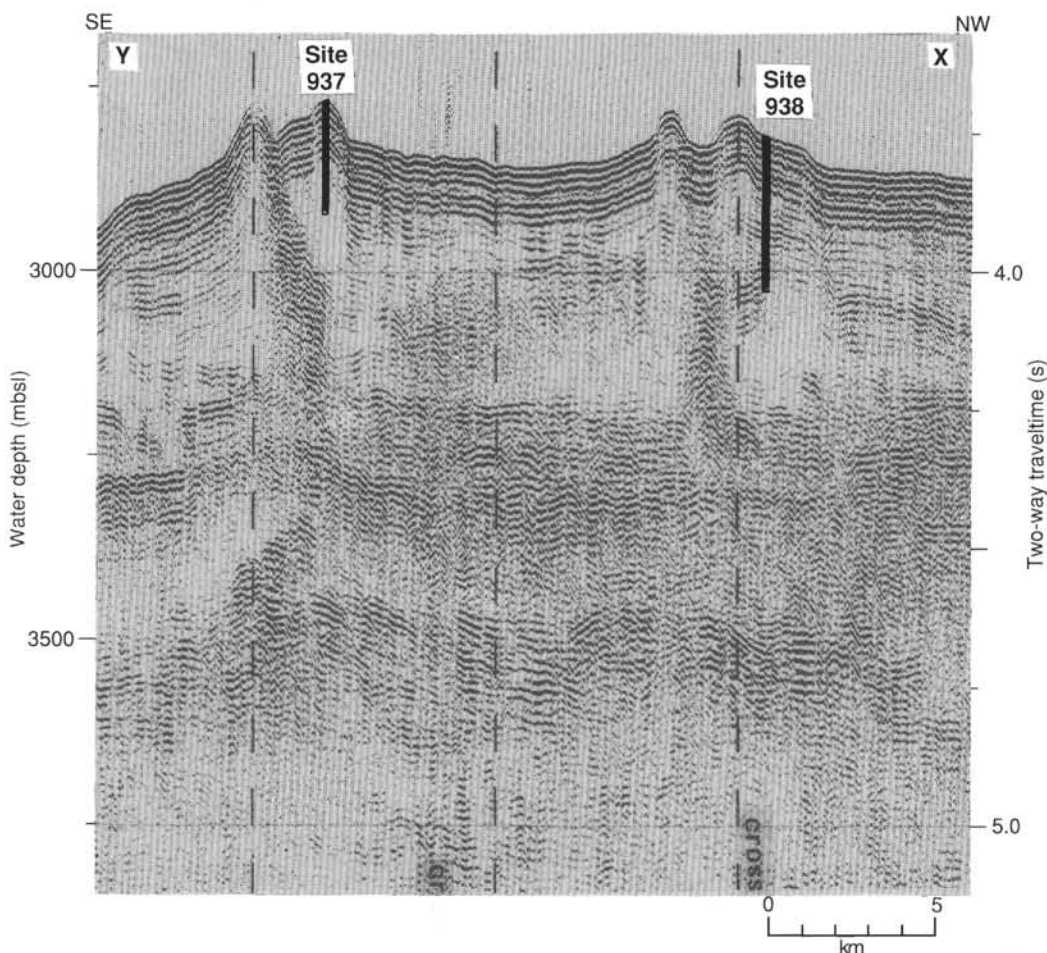


Figure 2. Seismic section through Site 937 (Profile X-Y; *Farnella*).

The site was selected from a *Farnella* seismic profile (FR815; 0758 hr on 12 Jan. 1982; Fig. 2). Our pre-site 3.5-kHz survey showed that the position selected on the narrow eastern (right) levee had a hyperbolic echo pattern suggesting slumping or other small-scale relief (Fig. 3). The site was moved to the western (left) levee (Fig. 3). The new position is equivalent to 0808 hr on the *Farnella* seismic line (Fig. 2).

The surficial sediment at the site, interpreted from 3.5-kHz sub-bottom profiles, is acoustically stratified, and a layer more than 10 ms thick is draped over the Yellow levee crest (Fig. 3). The actual crest of the Yellow levee crest is not seismically imaged at this site, but the levee flanks are imaged in seismic data to the east and west of the site (Fig. 2).

Objectives

The principal objectives at Site 937 were:

1. To sample the anticipated hemipelagic stratigraphic section above the Yellow levee on the eastern side of the fan to determine past changes in ocean circulation and to aid in determining the stratigraphy of the fan sediment.
2. To sample the sediment of the Yellow System in an upper fan setting. The Yellow System was studied in deeper water at Site 933.

OPERATIONS

Transit: Site 936 to Site 937 (AF-17)

The 59-nmi transit from Site 936 to Site 937 took 6.1 hr. We conducted a single-channel seismic-reflection survey over Site 938 (AF-16) and then pulled in the seismic gear and conducted a 3.5-kHz PDR survey over Site 937. The ship returned to 4°35.75'N, 47°12.45'W and deployed a beacon at 1115 hr 27 April. A BHA similar to that used at Site 936 was assembled and run to the seafloor.

Hole 937A

We positioned the bit at 2762.0 mbrf and spudded Hole 937A at 1620 hr 27 April. Core 1H recovered 0.21 m, and the mud line was defined to be at 2771.3 mbrf. The distance from sea level to rig floor, which depends on the ship's draft, was 11.14 m for Holes 937A and 937B, and 11.17 for Holes 937C and 937D. A good mud line was obtained, but a more complete mud-line core was desired, so this short core was archived as Hole 937A.

Hole 937B

We positioned the bit at 2769.0 mbrf, without moving the ship, and spudded Hole 937B at 1700 hr 17 April. Core 1H recovered 7.53

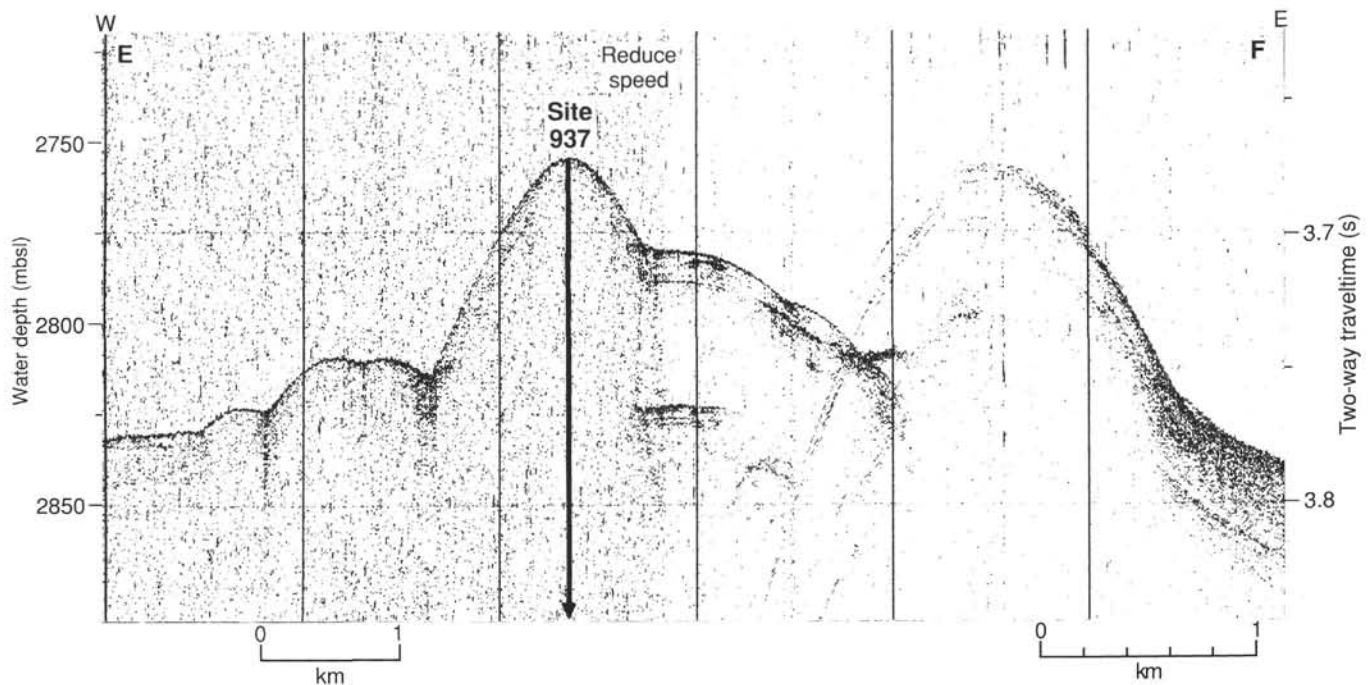


Figure 3. A 3.5-kHz profile through Site 937 (Profile E-F; JOIDES Resolution).

m (which was later corrected to 7.57 m, accounting for expansion), and the mud line defined to be at 2771.0 mbrf (Table 1). Cores 1H through 9H were taken from 2771.0 to 2854.5 mbrf (0–83.5 mbsf) and recovered 87.51 m (104.8%). Cores 3H through 9H were oriented using the Tensor tool. ADARA heat-flow measurements were taken during Cores 6H and 9H.

XCB Cores 10X through 19X were taken from 2854.5 to 2951.3 mbrf (83.5–180.3 mbsf), coring 96.8 m and recovering 71.69 m (74.1%). Parts of Cores 1H, 4H, 6H, 7H, and 11X were disturbed due to gas-induced extrusion of core out of the liner onto the rig floor or collapsed core liners. The pipe was pulled above the seafloor at 1135 hr 28 April.

Hole 937C

We moved the ship 20 m north, positioned the bit at 2767.0 mbrf, and spudded Hole 937C at 1220 hr 28 April. Core 1H recovered 9.05 m, and the mud line was defined to be at 2767.5 mbrf. Cores 1H through 8H were taken from 2767.5 to 2843.0 mbrf (0–75.5 mbsf) and recovered 80.52 m (106.6%). Cores 3H through 8H were oriented, and no heat-flow measurements were taken.

Increasing gas voids in Hole 937B led us to try using the Pressure Core Sampler (PCS). Although the clay was not yet stiff enough to recover with the XCB, we decided to run the PCS in an attempt to obtain a pressurized sample at in-situ pressures. Core 9P was taken at 2843.0–2844.0 mbrf (75.5–76.5 mbsf), but no sediment was recovered. The 1.0-m-long core was cut in 2 min with 8000-lb weight-on-bit (wob) at 80 rpm with 125–250 amps torque circulating a minimal 50 gpm at 125 psi. The ball valve was operated (closed) twice. Some pressure was trapped (~3700 psi; below hydrostatic for this depth), the ball valve had closed, and no core was recovered. There was no indication that core had ever entered into the bit throat or diaphragm catcher. When the ball valve assembly was removed, muddy water was released.

The bit was pulled above the seafloor at 1915 hr 28 April.

Hole 937D

We moved the ship 20 m north, positioned the bit at 2766.0 mbrf, and spudded Hole 937D at 1940 hr 28 April. Core 1H recovered 7.20 m, and the mud line was defined to be at 2768.3 mbrf. Cores 1H and 2H were taken from 2768.3 to 275.5 mbrf (0–16.7 mbsf) and recovered 17.26 m (103.4%). No core orientation or heat-flow measurements were taken. The pipe was pulled above the seafloor at 2045 hr 28 April, and we recovered the beacon. We then pulled the pipe up to 2674.1 mbrf in preparation for the dynamic positioning transit to Site 938.

LITHOSTRATIGRAPHY

Introduction

Four holes were drilled at Site 937 on the crest of the eastern levee of the Yellow Channel-levee system (Hole 937A, 0 to 0.2 mbsf; Hole B, 0 to 180.3 mbsf; Hole C, 0 to 76.5 mbsf; Hole D, 0 to 16.7 mbsf). Because there are no apparent differences between equivalent intervals in the four holes, the following lithologic description is based mainly on cores from the longest hole, Hole 937B (Fig. 4). Expansion of methane gas during core recovery commonly affected the sediment by disrupting the primary sedimentary structures in many silt and sand beds, and by producing void spaces within many of the core sections (see “Lithostratigraphy” section in the “Explanatory Notes” chapter, this volume). The sedimentary section is divided into Units I and II. Unit II is further subdivided into four subunits (Figs. 4 and 5).

Description of Lithostratigraphic Units

Unit I

Intervals: 155-937A-1H-1, 0–20 cm; 155-937B-1H-1, 0–85 cm; 155-937C-1H-1, 0–85 cm; 155-937D-1H-1, 0–95 cm

Table 1. Site 937 coring summary.

Core	Date (1994)	Time (UTC)	Depth (mbsf)	Length cored (m)	Length recovered (m)	Recovery (%)
155-937A-1H	April 27	2035	0.0-0.2	0.2	0.21	100.0
Coring totals				0.2	0.2	100.00
155-937B-						
1H	April 27	2110	0.0-7.5	7.5	7.57	101.0
2H	April 27	2150	7.5-17.0	9.5	10.26	108.0
3H	April 27	2230	17.0-26.5	9.5	10.27	108.1
4H	April 27	2315	26.5-36.0	9.5	9.80	103.0
5H	April 27	2355	36.0-45.5	9.5	10.13	106.6
6H	April 28	0100	45.5-55.0	9.5	10.34	108.8
7H	April 28	0145	55.0-64.5	9.5	9.21	96.9
8H	April 28	0235	64.5-74.0	9.5	9.68	102.0
9H	April 28	0335	74.0-83.5	9.5	10.25	107.9
10X	April 28	0445	83.5-93.0	9.5	4.96	52.2
11X	April 28	0550	93.0-102.7	9.7	9.76	100.0
12X	April 28	0650	102.7-112.4	9.7	8.29	85.4
13X	April 28	0755	112.4-122.1	9.7	8.14	83.9
14X	April 28	0850	122.1-131.8	9.7	8.76	90.3
15X	April 28	0945	131.8-141.5	9.7	6.60	68.0
16X	April 28	1055	141.5-151.2	9.7	4.23	43.6
17X	April 28	1200	151.2-160.9	9.7	8.56	88.2
18X	April 28	1305	160.9-170.6	9.7	3.30	34.0
19X	April 28	1425	170.6-180.3	9.7	9.60	98.9
Coring totals				180.3	159.7	88.60
155-937C-						
1H	April 28	1630	0.0-9.0	9.0	9.07	101.0
2H	April 28	1710	9.0-18.5	9.5	10.18	107.1
3H	April 28	1800	18.5-28.0	9.5	10.40	109.5
4H	April 28	1840	28.0-37.5	9.5	10.38	109.2
5H	April 28	1920	37.5-47.0	9.5	10.36	109.0
6H	April 28	2000	47.0-56.5	9.5	10.26	108.0
7H	April 28	2045	56.5-66.0	9.5	9.82	103.0
8H	April 28	2125	66.0-75.5	9.5	10.05	105.8
9P	April 28	2235	75.5-76.5	1.0	0.00	0.0
Coring totals				76.5	80.5	105.20
155-937D-						
1H	April 28	2350	0.0-7.2	7.2	7.20	100.0
2H	April 29	0025	7.2-16.7	9.5	10.06	105.9
Coring totals				16.7	17.3	103.30

Note: An expanded version of this coring summary table that includes lengths and depths of sections, location of whole-round samples, and comments on sampling disturbance is included on the CD-ROM in the back pocket of this volume.

Age: Holocene
Depth: 0-0.85 mbsf

Unit I consists of nannofossil-foraminifer clay and foraminifer-nannofossil clay, which grades downward to nannofossil-rich clay or nannofossil-rich silty clay with a transitional color change from yellowish brown (10YR 5/4; 0-0.38 mbsf) through grayish brown (2.5Y 5/2) and gray (5Y 5/1) (0.38-0.55 mbsf), to dark gray (5Y 4/1) (0.55-0.85 mbsf). The sediment is moderately bioturbated and contains four indurated brown (10YR 5/3) to grayish brown (10YR 5/2) crusts (at intervals 937B-1H-1, 15-18 cm, 22-23 cm, 20-29 cm, and 37-38 cm). Only two crusts occur in Holes 937C and 937D. The lowest crust is the most distinct and corresponds to a similar diagenetic iron-rich crust recovered at most Leg 155 sites. Similar iron-rich crusts were analyzed previously and correlated throughout the Amazon Fan and adjacent Guiana Basin (Damuth, 1977; see "Introduction" chapter, this volume). The carbonate content of Unit I decreases rapidly downhole from 47.7% at 0.2 mbsf to 7.9% at 0.48 mbsf (see "Organic Geochemistry" section, this chapter); the high carbonate values are associated with the nannofossil-foraminifer clay that forms the upper part of the unit.

Unit II

Intervals: 155-937B-1H-1, 85 cm, through -19X; 155-937C-1H-1, 85 cm, through -8H; 155-937D-1H-1, 95 cm, through -2H

Age: Holocene to late Pleistocene
Depth: 0.85-180.30 mbsf

Unit II includes the entire recovered section below Unit I and consists mainly of terrigenous, dark gray (5Y 4/1) to very dark gray (5Y 3/1) clay and silty clay. Four subunits are recognized, based on the downhole appearance and then the subsequent increase in the frequency and thickness of laminae and thin beds of silt (Fig. 5). Unit II is characterized by ubiquitous faint mottling related to moderate burrowing and bioturbation. The burrows are highlighted by the presence of hydrotroilite staining. Locally, hydrotroilite also forms thin dark color bands spaced at intervals of approximately 1-3 cm. Where the color bands are more closely spaced than 1 cm, they resemble varves (Fig. 6). The color banding is related to alternating laminae of silty clay and clayey silt; the more silt-rich layers have lighter color. Millimeter-scale, scattered, soft micronodules thought to be hydrotroilite are common to very abundant in some intervals. Laminae and beds of silt and very fine sand are also commonly stained by disseminated hydrotroilite (see "Introduction" chapter, this volume).

Subunit IIA

Subunit IIA extends from 0.85 to 10.50 mbsf (interval 937B-1H-1, 85 cm, through -2H-2, 150 cm) and consists of a dark gray (5Y 4/1) to dark olive gray (5Y 3/2) terrigenous clay grading downhole to silty clay. Carbonate content is about 0.1%. Black (N2) color mottling is extensive and appears as common and very irregular patches in the split cores. The irregular mottling is thought to correspond to bioturbated sediment. Most black (N2) color bands are restricted to the lower part of the subunit. The base of Subunit IIA is a 2.30-m-thick black color band (from 8.20 to 10.50 mbsf) with upper and lower contacts that dip at 65° and 80°, respectively. This band also occurs in Hole 937C (from 5.80 to 8.80 mbsf), where it contains hydrotroilite nodules with dimensions of tens of centimeters. The equivalent interval in Hole 937D contains intense hydrotroilite mottling. The steeply dipping boundaries of the black band in Hole 937B are thought to correspond to near-surface steep normal faults (e.g., in interval 937C-3H-4, 10-90 cm), where a steeply dipping surface off-sets color mottles.

Subunit IIB

Subunit IIB extends from 10.50 to 34.73 mbsf (Section 937B-2H-2, 150 cm, through -4H-6, 73 cm) and consists predominantly of homogeneous dark gray (5Y 4/1) silty clay. There are scattered, soft, black (N2) hydrotroilite micronodules. Faint color mottling suggests slight to moderate disturbance by burrowing organisms. Rare, 2-mm-diameter, pale blue vivianite patches characterize all but the first section of Core 937B-3H. Carbonate content is about 1.5%.

Subunit IIC

The boundary between Subunit IIB and Subunit IIC is placed at the first reappearance of color banding, just below a 2.15-m-thick interval with abundant soft hydrotroilite micronodules. Subunit IIC extends from 34.73 to 93.51 mbsf (interval 937B-4H-6, 73 cm, through -11X-2, 23 cm) and consists predominantly of dark gray (5Y 4/1) to very dark gray (5Y 3/1), faintly mottled silty clay (Fig. 7). There are common laminae and 1- to 3-cm-thick beds of silt. Carbonate content is uniformly low throughout Subunit IIC at about 2.5%.

Most silt beds in Subunit IIC have an upper parallel-laminated division (Fig. 6). A few beds show parallel laminations throughout. Cross-lamination is rare (Fig. 8). On average, fewer than four laminae or thin beds of silt occur per meter of core. The frequency and thickness of silt layers are not uniform downhole, but define three fining-upward cycles (interval 937B-4H-6, 73 cm, through -6H-4, 128 cm; interval 937B-6H-4, 128 cm, through -9H-1, 59 cm; interval 937B-9H-1, 59 cm, through -9H-CC). Silt laminae and thin silt beds are absent from the upper part of each cycle and increase to approximately eight per meter of core in the lower part of each cycle (Fig. 9).

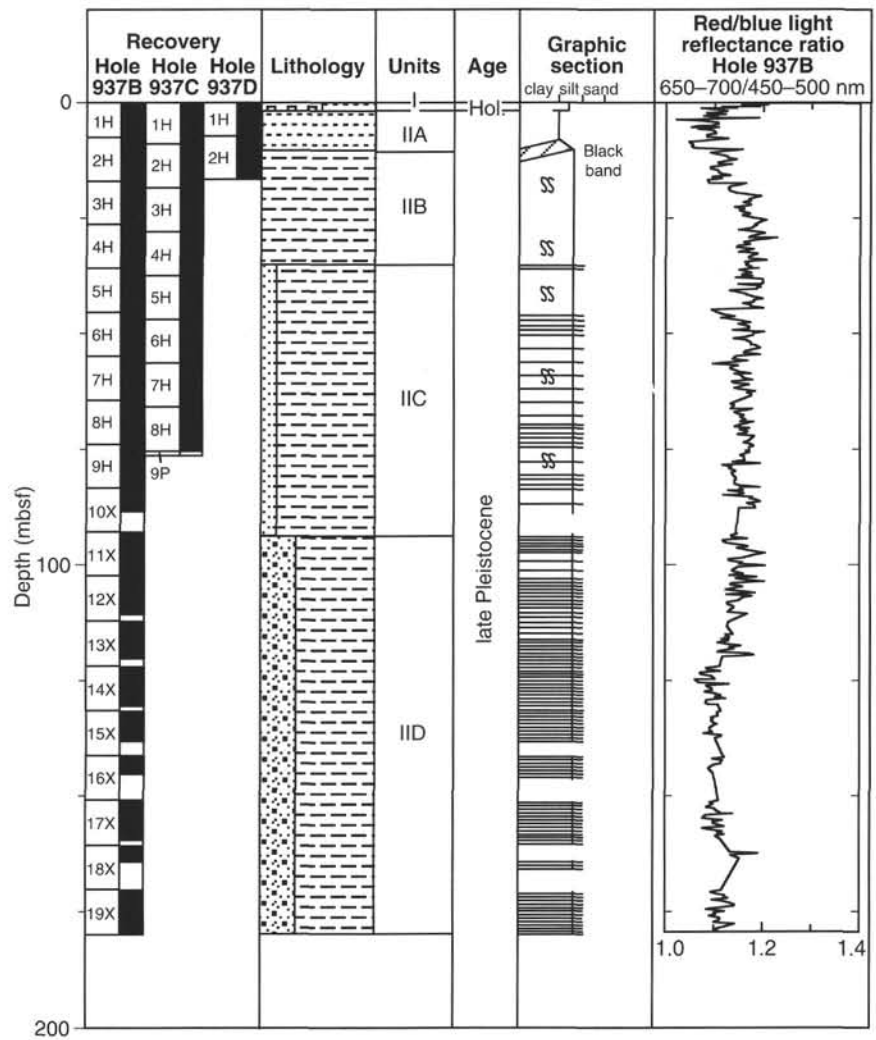


Figure 4. Composite stratigraphic section for Site 937 showing core recovery in all holes, a simplified summary of lithology, depth of unit boundaries, age, a graphic section with generalized grain-size and bedding characteristics, and downhole variations in light-reflectance values for cores from Hole 937B only. The lithologic symbols are explained in Figure 1 of the "Explanatory Notes" chapter, this volume.

This cyclicity indicates either lateral shifts in the loci of silt deposition and/or a temporal decrease in the frequency or size of turbidity currents.

Burrows are particularly evident in the lower part of the uppermost cycle, commonly highlighted because they mix contrasting colors of sediment across the top of silt beds (interval 937B-5H-2, 47 cm, through -6H-4, 128 cm). The burrows appear as 1- to 2-cm-thick bands or ellipses crossing the split cores horizontally, or with a slight inclination (5° to 20° dip), and contain curved backfill laminae (*Spreiten*). Some of the burrows resemble echinoid burrows in size and shape (Fig. 7 and 8), an interpretation supported by the presence of echinoid spines (see "Biostratigraphy" section, this chapter).

Subunit IID

Subunit IID extends from 93.51 mbsf to the bottom of Hole 937B at 180.20 mbsf (interval 937B-11X-2, 23 cm, through -19X-CC). The sediment consists predominantly of dark gray (5Y 4/1) to very dark gray (5Y 3/1) faintly mottled silty clay with laminae and beds of silt and very fine sand. Silt and very fine sand layers are more abundant than in Subunit IIC. Most silt beds either contain laminae of mud in their upper part, or are laminated throughout. The carbonate content is uniformly low throughout Subunit IID and averages about 2.5%.

The upper limit of Subunit IID marks the start of a moderate downhole increase in laminae and beds of silt and very fine sand, which increase in frequency from six to more than 30 per meter of

core. About 70% of these layers are 1- to 3-cm-thick silt beds. These beds represent about 20%–30% of the volume of the sedimentary succession. Beds 5–10 cm thick are less common and compose 10% of the coarser grained layers. The remaining 20% of the coarse fraction is thin laminae of fine to medium silt with sharp bases and tops, and no recognizable lamination. Many of the beds of silt and fine sand, as well as some of the thick silt laminae, appear normally graded with sharp bases and gradational tops. A few beds have irregular bases. Some beds grade upward from fine sand through silt into alternating 1-mm-thick laminae of silt and mud, and finally into mud (Fig. 6). Cross-lamination is evident in approximately 5% of the beds.

Discontinuous/disrupted silt and sand laminae (Fig. 10) characterize cores below Section 937B-17X-2 at 70 cm, thought to be a result of sediment shearing by rotation during XCB drilling (see "Lithostratigraphy" section, "Explanatory Notes" chapter, this volume). However, the sediment may have been naturally deformed; drilling disturbance may have only enhanced existing features. The disrupted sediment could have been formed by boudinage and tilting of these silt layers during differential mass movement. The occurrence of extraformational carbonate-rich mud clasts in Core 937B-17X supports this hypothesis.

The carbonate-rich clasts were observed in Subunit IIC at interval 937B-9H-4, 67–68 cm, and in Subunit IID at intervals 937B-15X-2, 37–38 cm, and -17X-3, 43–44 cm (Fig. 11). Clasts appear as centimeter-size, elongate to irregularly shaped, olive (5Y 4/3) to brown

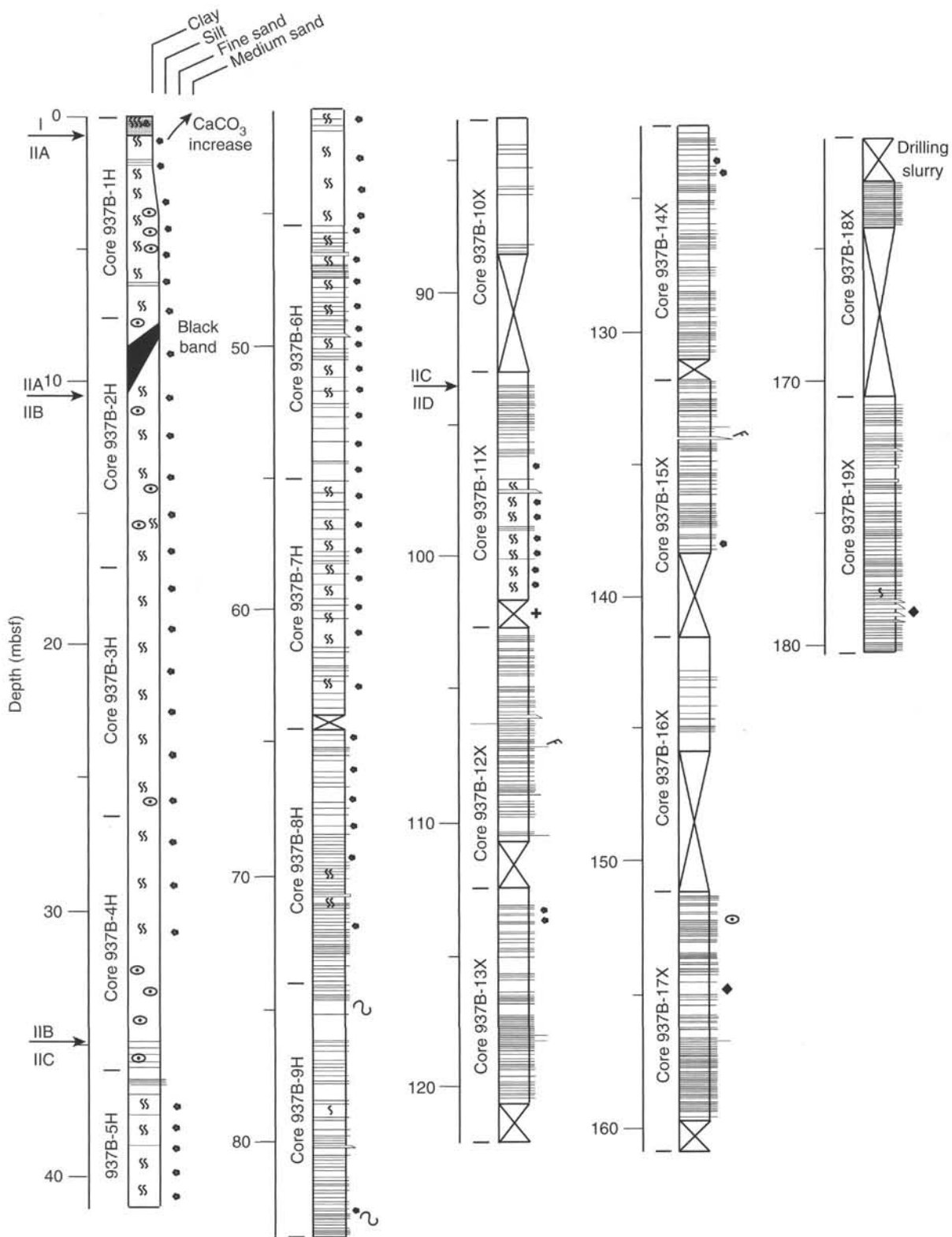


Figure 5. Graphic sedimentological columns for Site 937 showing grain-size variation (width of columns), bed thickness, and sedimentary structures; symbols and preparation of these columns are explained in the "Lithostratigraphy" section of the "Explanatory Notes" chapter, this volume. Arrows indicate the positions of unit and subunit boundaries. The upper part of the column is shown in the strike section of the foldout (back pocket, this volume) for comparison of levee sequences on the middle and upper fan.

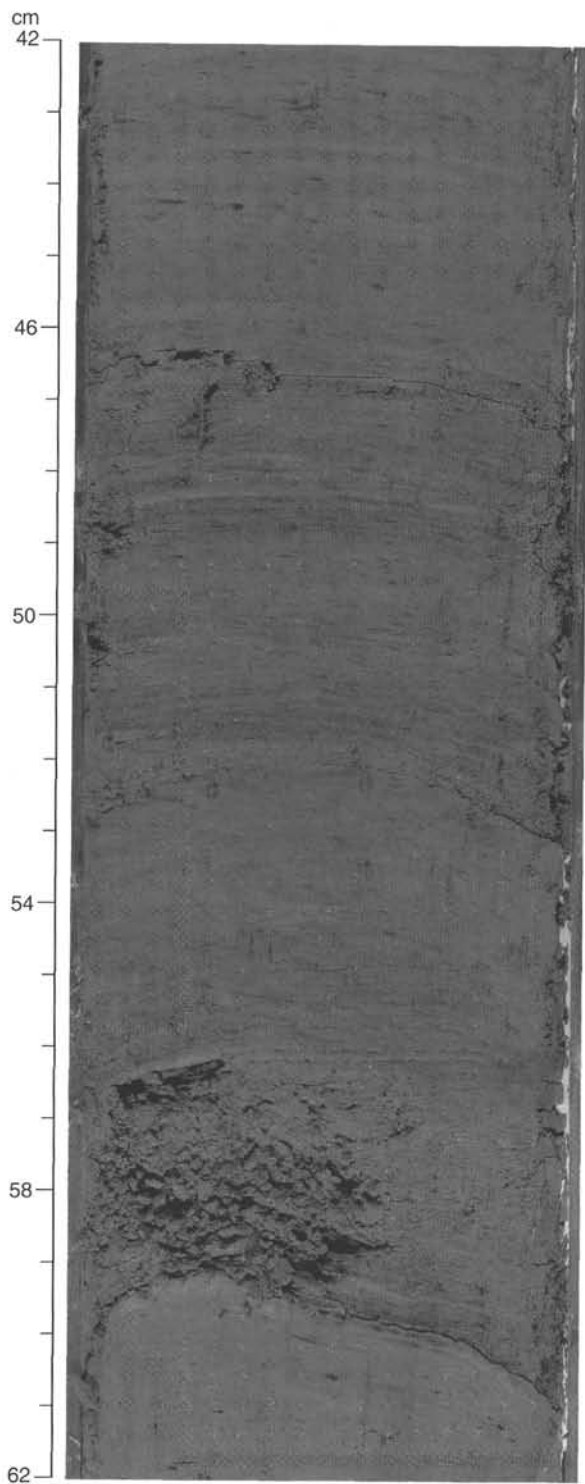


Figure 6. Example of a graded muddy turbidite. The bed has a sharp base (60 cm) and transitional top. From bottom to top, the bed exhibits 3 cm of massive, coarse silt, overlain by 10 cm of mm-thick interlaminae of silt and silty clay, overlain by color-banded silty clay (interval 155-937B-9H-1, 42–62 cm).

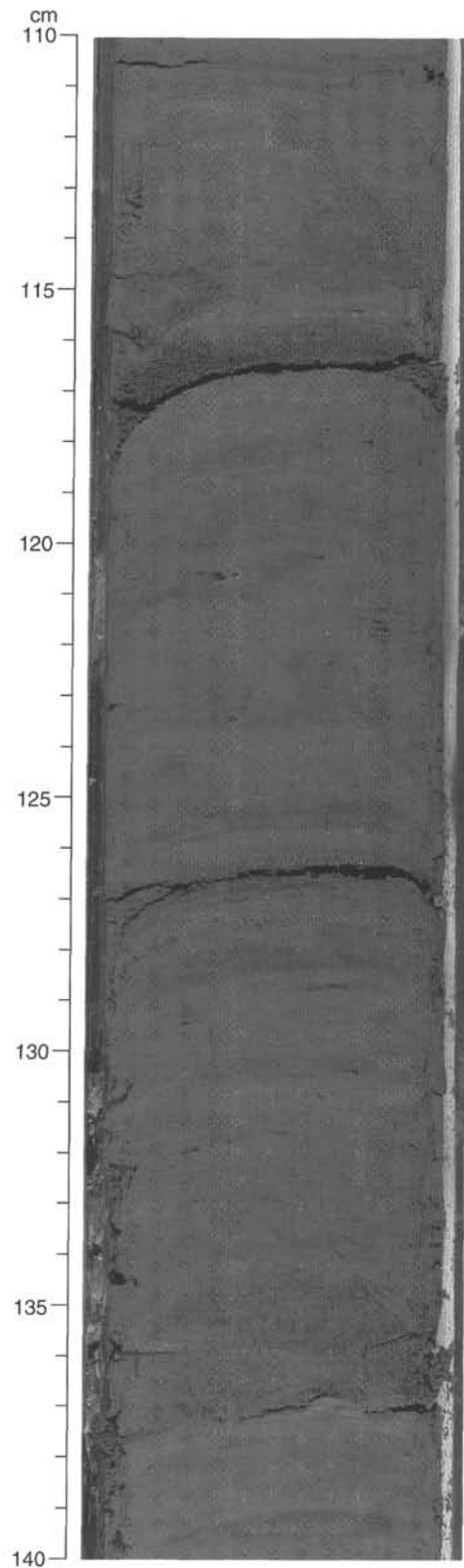


Figure 7. Slightly color-banded and mottled silty clay of Subunit IIC (interval 155-937C-6H-3, 110–140 cm). The mottling is related to intense burrowing (e.g., 112–116 cm and 134–136 cm).

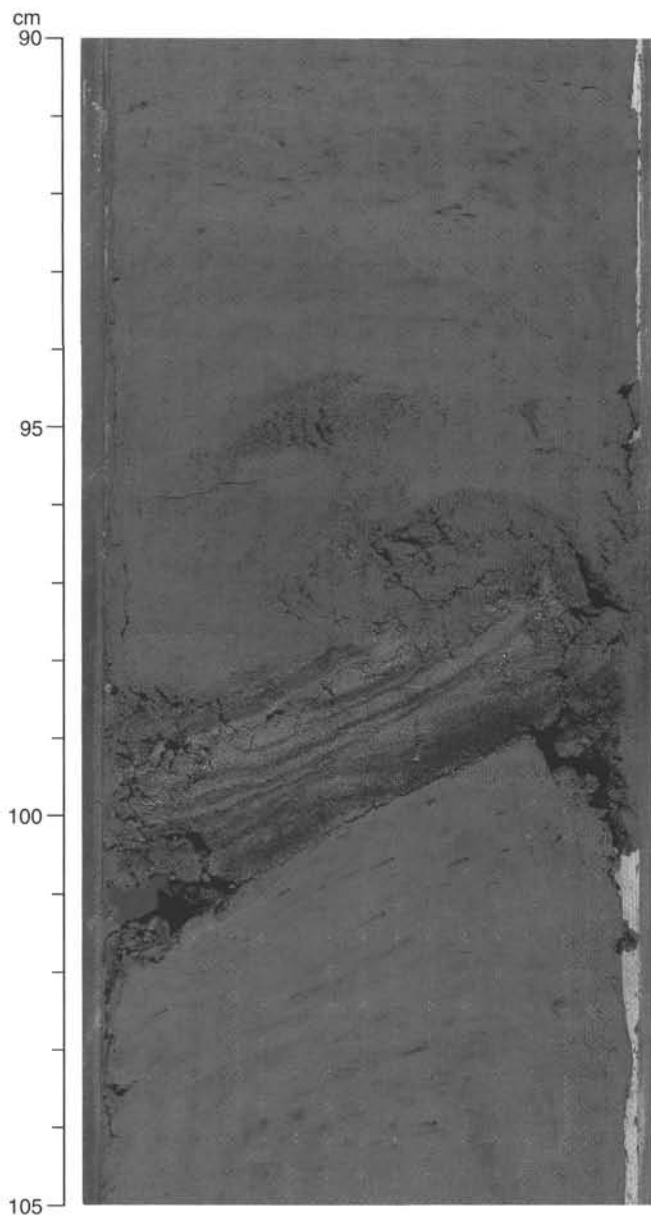


Figure 8. Cross-laminated, coarse silt bed in bioturbated and slightly mottled silty clay of Subunit IIC (interval 155-937C-7H-6, 90–105 cm). The alternating dark and light lamination is attributable to variations in content of organic detritus. The bed has a sharp base and top. The silt is inferred to have been transported by highly tractional turbidity currents. The top of the bed is in part (right half) disrupted by a large burrow of an echinoid(?), which displays an ellipsoidal shape and internal *Spreiten*.

(10YR 5/3) calcareous clay with a few nannofossils that show considerable dissolution and overgrowth. The clast in Figure 11 is associated with a soft nodule (23.9% carbonate) that contains common brown foraminifers and unusually common white pteropods, and some vivianite (see “Biostratigraphy” section, this chapter). X-ray diffraction analysis of the nodule shows siderite but no detectable calcite, suggesting the complete substitution of the calcareous skeletal fraction by siderite, accounting for the brown color of the foraminifers. The presence of abundant pteropods suggests that this sediment was re-deposited from shallow water, probably as a calcareous-rich clast, which then acted as a nucleus for siderite precipitation.

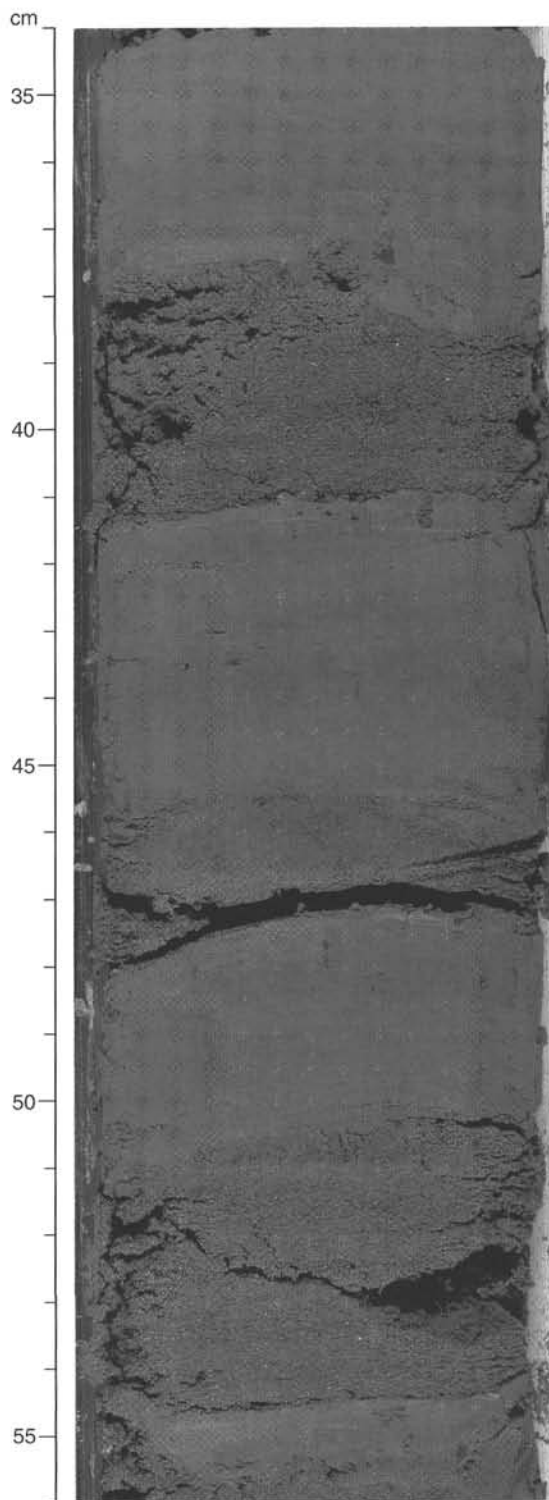


Figure 9. Structureless, closely spaced, 1- to 4-cm-thick, coarse silt beds alternating with slightly mottled and bioturbated silty clay (interval 155-937C-6H-3, 34–56 cm). Beds have sharp bases and tops.

Mineralogy

Mineralogy was determined by estimation of mineral volume percentages in smear slides, and by X-ray diffraction (XRD) analysis of clay, silt, and sandy silt layers.

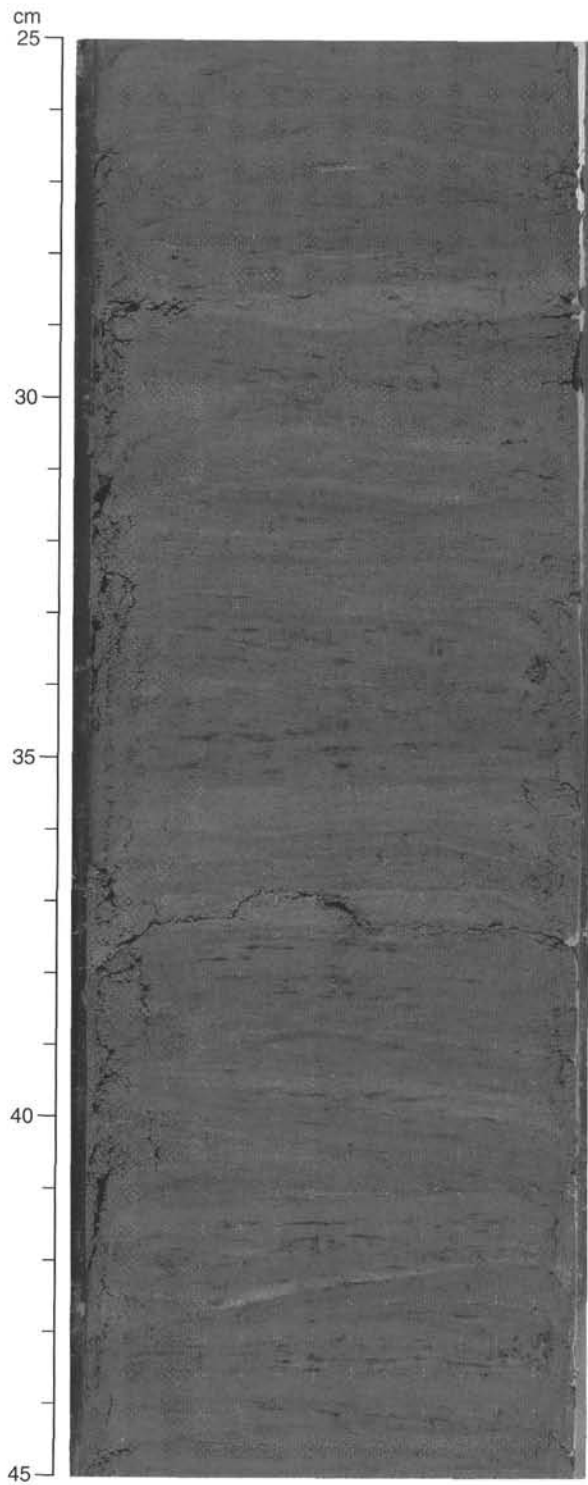


Figure 10. “Wispy” and disrupted silt laminae and thin silt beds in Subunit IID (interval 155-937B-19X-7, 25–45 cm). This facies is segmented into “biscuits” induced by XCB rotary drilling.

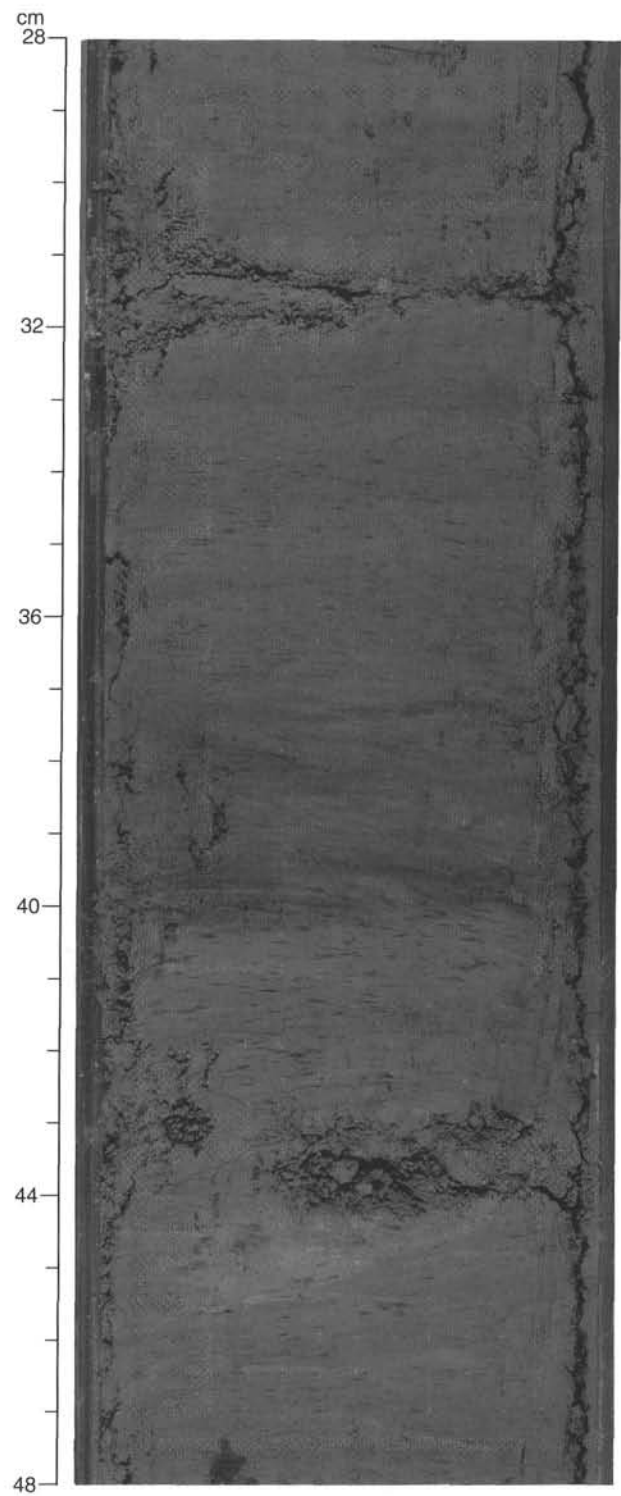


Figure 11. Irregular clast of olive (5Y 4/3), calcareous clay at 43–44 cm from Subunit IID (interval 155-937B-17X-3, 28–48 cm). This clast is associated with a soft, brown (10YR 5/3) siderite nodule and is inferred to have acted as a nucleus for siderite precipitation. A similar colored zone is at 31–32 cm.

Table 2. Relative peak intensities of the main minerals in representative lithologies at Hole 937B.

Core, section, interval (cm)	Lithology	Depth (mbsf)	Relative intensity of primary peaks								
			Smectite	Mica + Illite	Kaolinite	Quartz	Plagioclase	K-feldspar	Augite	Hornblende	Calcite
155-937B-											
1H-1, 10-11	Carbonate clay	0.10	18.0	10.7	10.7	100.0	10.2	*	*	*	222.7
1H-1, 90-91	Silty clay	0.90	4.6	16.1	8.2	100.0	7.6	*	3.5	*	1.7
1H-5, 118-119	Silty clay	7.18	14.7	23.7	17.4	100.0	10.5	*	2.9	*	*
2H-1, 110-111	Silty clay	8.60	15.2	24.4	14.9	100.0	11.2	*	4.1	*	*
2H-6, 56-57	Silty clay	15.56	18.8	28.7	18.2	100.0	10.8	*	3.4	*	*
3H-4, 40-41	Silty clay	21.90	13.7	25.0	13.7	100.0	15.0	*	3.2	2.8	*
4H-7, 50-51	Silty clay	36.00	8.2	24.3	12.7	100.0	11.1	5.6	3.1	*	*
5H-4, 108-109	Silty clay	41.58	6.6	13.8	10.5	100.0	9.2	*	2.5	*	*
6H-4, 23-24	Silt	49.91	1.7	4.8	2.5	100.0	10.5	3.1	0.9	*	*
7H-2, 103-104	Silt	56.32	2.9	3.6	2.5	100.0	11.0	4.4	1.0	*	*
8H-5, 19-21	Silt	69.51	10.1	17.3	9.1	100.0	10.9	4.9	1.5	2.0	*
9H-3, 85-86	Silt	77.85	8.4	17.0	9.3	100.0	12.2	3.9	1.4	*	*
10X-2, 121-122	Silt	86.21	4.1	6.9	4.2	100.0	11.3	4.3	1.9	0.9	*
11X-2, 50-51	Silt/clay	93.78	3.8	9.5	4.8	100.0	8.3	*	1.6	*	*
12X-5, 10-12	Fine sand/silt	108.80	2.6	4.8	2.7	100.0	10.1	3.9	1.1	*	*
13X-2, 110-111	Silt	115.00	10.5	20.5	8.7	100.0	10.5	*	2.2	*	*
13X-4, 98-99	Fine sand/silt	117.88	2.3	6.2	3.3	100.0	10.7	3.3	0.9	0.7	*
14X-6, 6-7	Silt	129.66	6.9	10.0	4.5	100.0	9.1	5.9	1.6	*	*
15X-4, 41-42	Silt	136.71	6.7	12.7	5.8	100.0	11.7	8.6	1.0	0.8	*
16X-3, 49-50	Silt	144.99	9.0	14.4	7.9	100.0	10.5	4.8	2.3	2.2	*
17X-4, 92-93	Fine sand	156.62	2.3	6.2	3.1	100.0	8.9	3.5	1.5	1.8	*
18X-2, 118-119	Silt	163.58	5.4	10.3	5.7	100.0	11.4	3.2	1.4	1.1	*
19X-2, 62-63	Silt	172.72	3.2	8.7	3.9	100.0	8.6	4.0	0.9	1.3	0.8

Notes: See "Lithostratigraphy" section in the "Explanatory Notes" chapter, this volume, for XRD methods. * denotes non-detection.

Smear-slide Synthesis

Silty clay, the dominant lithology at this site, contains 23%–40% medium to fine silt (5 to 25 μ m) consisting of 30%–75% quartz (mainly monocrystalline), 3%–25% feldspar, 3%–10% mica, and 6%–30% accessory minerals. The accessory minerals are mainly green hornblende, pyroxene, and opaque minerals dispersed in the mud or contained in thin laminae (0.25–1 mm thick). Plant debris is commonly present in Subunits IIC and IID and forms 10% of the sediment in Sample 937B-12X-1, 80–81 cm. Diagenetic accessory minerals include widespread black hydrotroilite and blue vivianite.

Laminae and beds of medium to coarse silt and fine sand consist of relatively well-sorted, angular grains of quartz (~30%), feldspar (~25%), rock fragments (~25%), mica (~8%), and accessory minerals (~12%). The accessory minerals include amphibole (mainly hornblende), augite, zircon, and opaque minerals. The silt laminae commonly contain a hydrotroilite-rich clay-sized fraction (5% to 30%). The feldspar and ferromagnesian minerals are very fresh, indicating rapid transport and burial. In contrast, some of the larger quartz grains are well-rounded with surface coatings of iron oxides/hydroxides. These features suggest exposure under lateritic-weathering conditions and prolonged transport.

XRD Data

Bulk XRD analysis was performed on samples of a carbonate clay from Core 937B-1H, seven silty clays from Cores 937B-1H through -5H, and silt and fine sand from most cores below 45 mbsf (Table 2; Fig. 12). The common minerals throughout the cored succession, based on the relative intensities of their primary peaks (normalized to quartz intensity), are quartz, plagioclase, K-feldspar, augite, and the clay minerals smectite, illite (+ mica), and kaolinite. A few samples contain calcite and an amphibole that is probably hornblende based on its presence in smear slides.

The clay mineral with the highest relative peak intensity is illite (+ mica). In silty clay samples, the relative abundance of all clay minerals increases from 0 to 15 mbsf and then decreases from 15 to 55 mbsf (Fig. 12A). This effect is most apparent in the illite (+ mica) intensities. Deeper than 45 mbsf, micas likely account for fluctuations in the relative intensity of clay minerals + micas in the silt and fine sand samples. Given the semi-quantitative character of our data (see "Lithostratigraphy" section, "Explanatory Notes" chapter, this vol-

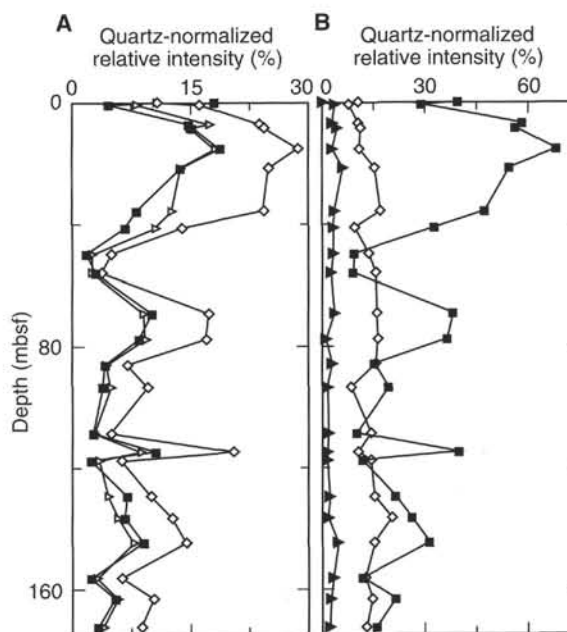


Figure 12. Relative abundances of silicate minerals in representative samples, based on XRD analysis (Table 2). **A.** Plot against depth of relative peak intensities of clay minerals + micas by core number. Squares = smectite; diamonds = illite (+ mica); triangles = kaolinite. **B.** Plot against depth of relative peak intensities of major mineral groups by core number. Squares = clay minerals + micas; diamonds = feldspar; and small triangles = augite + hornblende.

ume), there appears to be no significant downhole variation in the relative abundances of feldspars, hornblende, and augite, regardless of grain size (Fig. 12A).

Spectrophotometry

Light reflectance levels of sediment in Unit II never exceed 25% in the wavelength band from 400 to 700 nm because of the general dark gray to very dark gray color of the sediment. For the calcareous

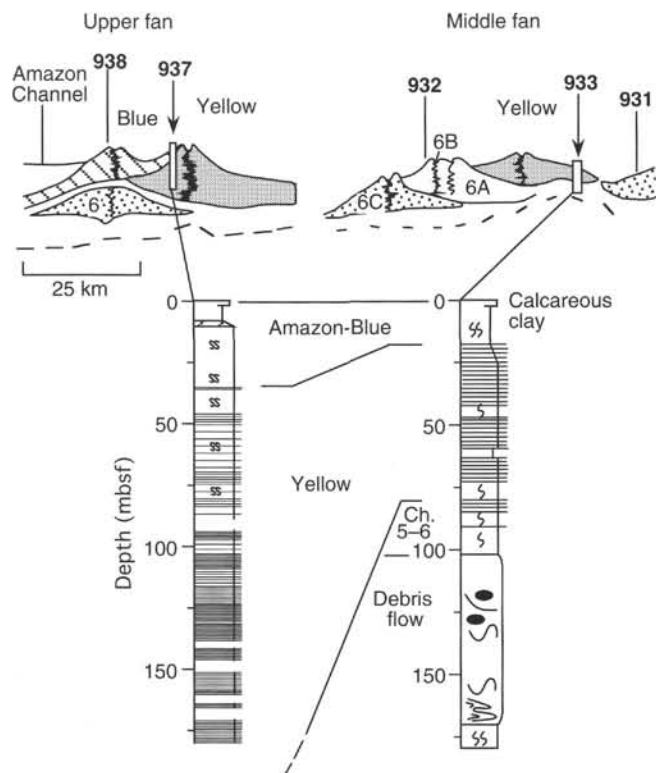


Figure 13. Comparison of lithology from the Yellow Channel-levee System at Site 937 (upper fan) and Site 933 (middle fan).

clay of Unit I, highest reflectance values reach 35%. The ratio between red (650–700 nm) and blue (450–500 nm) spectral reflectance averages 1.14 (Fig. 4). The highest red/blue ratio is related to the brownish gray calcareous clay of Unit I, reflecting the enhancement of red reflectance caused by iron oxyhydroxides. The lowest red/blue ratio corresponds to the 2.30-m-thick black color band at the base of Subunit IIA (8.20 to 10.50 mbsf).

The downhole changes in the red/blue ratio throughout Unit II are not related to changes in the primary lithologies (clay, silt laminae or beds); the high-frequency variability probably results from the irregular intensity of black color mottling and banding, which is related to the diagenetic formation of hydrotroilite.

Discussion

Site 937 is located on the crest of the western levee of the Yellow Channel-levee System in the upper fan area (Fig. 13). The recovered section shows several possible fining- and thinning-upward muddy turbidite sequences in Subunits IIC and IID draped by bioturbated muds (Subunits IIA and IIB) that, in turn, are overlain by a hemipelagic interval (Unit I). The overall fining-upward sequence of Subunits IIC and IID, coupled with the abundance of burrowing in the upper part of this sequence, may be related to the autocyclic construction of the Yellow Channel-levee System, which increasingly constrained the coarse sediment fraction in the channel as it grew. However, the turbidite mega-sequence is composed of stacked fining-upward cycles (tens of meters thick) topped by bioturbated muds. These small cycles suggest short climate-related periods of fluctuating terrigenous influx during the buildup of the levee. The Yellow Channel-levee System was abandoned during deposition of the upper part of Subunit IIC, and the switch away from the Yellow System may have triggered the deposition of Subunit IIB. Subunit IIA may result from an even later shift of the active channel. Subunit IIB,

mainly composed of homogeneous silty clay, may have been deposited by settling of suspended mud originating from distant overspill along the Blue Channel-levee System. The color-banded clay of Subunit IIA may be related to the settling of suspended muds from the even more distant Amazon Channel.

The Yellow Channel-levee System has been cored in deeper water on the middle fan at Site 933, where it displays a thinner, muddy-turbidite sequence of superimposed fining-upward cycles grading into bioturbated intervals, which is similar to this site (Fig. 13). However, at Site 933, an overall fining-upward trend was not noted, perhaps because the hole penetrated a debris flow before reaching the deepest levels of the levee (Fig. 13).

BIOSTRATIGRAPHY

Calcareous Nannofossils

Nannofossils are abundant and well-preserved in the hemipelagic mud of Holocene age (Zone CN15b; Samples 937B-1H-1, 0–1 cm, through 937B-1H-1, 40 cm; Table 3). Below the “iron-rich crust” at 0.38 mbsf nannofossils become rare and poorly preserved, and Unit II is characterized by the low abundance or absence of calcareous nannofossils. The presence of *E. huxleyi* places Unit II in nannofossil Zone CN15b (Table 3). The nannofossil assemblages have a low diversity and are strongly affected by dissolution. Therefore, only more solution-resistant species are found (e.g., *Gephyrocapsa oceanica* and *Cyclococcolithus leptoporus*). Carbonate-rich clasts within Cores 937B-15X and -17X were found to be almost barren of nannofossils (e.g., Sample 937B-17X-3, 43 cm). These clasts consist of more than 95% carbonate particles and only a few poorly preserved nannofossils. As observed in previous sites, nannofossils tend to occur in slightly higher abundances in the top of turbidites (e.g., Sample 937B-9H-4, 67 cm).

Planktonic Foraminifers

The boundary between Ericson Zones Z and Y (disappearance of *G. tumida*) is preliminarily placed between Samples 937A-1H-CC, 6 cm (7.55 mbsf), and 937A-2H-CC, 37 cm (17.75 mbsf; Table 4). However, this interpretation is open to doubt given the possible downhole contamination of core-catcher samples. The Z/Y may thus be within Core 936-1H and hence shallower than 7.5 mbsf. The interval between the Z/Y boundary and 180.19 mbsf (Sample 937A-19X-CC, 1–10 cm), which corresponds to lithologic Unit II (Fig. 14), has been defined as the Y zone on the basis of the absence of *G. menardii* and *G. tumida*. This interval also can be constrained in age to less than 40 ka by the absence of *P. obliquiloculata*. Planktonic foraminifers are relatively abundant in Units I and IIA. In Subunit IIB, the bioturbated sediment is characterized by moderate abundance of planktonic foraminifers. Well-preserved echinoid spines are found sporadically in Subunits IIA, IIB, and IIC (Samples 937B-3H-CC, 28–37 cm [27 mbsf], 937B-6H-CC, 46–55 cm [56 mbsf], and 937B-7H-CC, 73–82 cm [64 mbsf]). Planktonic foraminifers have low abundances in lithostratigraphic Subunit IIC (Sample 937B-9H-CC, 67–75 cm [84 mbsf]). The bottom of Subunit IIC contains coarser grained sediment and abundant authigenic minerals (vivianite and iron sulfides). Planktonic foraminifer abundances are relatively low in Subunit IID (Samples 937B-11X-CC, 38–47 cm [102 mbsf], to 937B-19X-CC, 1–10 cm [180 mbsf]), which also contains abundant authigenic minerals, mica, and fine wood fragments. Aragonite pteropods are found throughout Unit II (Samples 937B-8H-CC, 34–43 cm [62 mbsf], 937B-10X-CC, 36–45 cm [88 mbsf], 937B-11X-CC, 38–47 cm [103 mbsf], 937B-14X-CC, 9–18 cm [131 mbsf], and 937B-17X-CC, 13–22 cm [160 mbsf]), and suggest that the low abundances of planktonic foraminifers are due to high sedimentation rates and not dissolution. Some iron-stained planktonic foraminifers

Table 3. Calcareous nannofossil and siliceous microfossil abundance data for Hole 937B.

Core, section, interval (cm)	Top interval (mbsf)	Bottom interval (mbsf)	Calcareous nannofossils			Diatoms				Ericson Zone (inferred from foraminifers)	Age (inferred from foraminifers)
			Abundance	Preservation	Zone	Marine	Freshwater	Sponge spicules	Radiolarians		
155-937B-											
1H-MI, 0		0.00	a	g	CN15b	vr	b	f	b	Z	Holocene
1H-1, 0-1	0.00	1.00	a	g		r	b	c	c		
1H-1, 9	0.09		a	g							
1H-1, 16	0.16		a	g							
1H-1, 24	0.24		c	g							
1H-1, 34	0.34		f	g							
1H-1, 40	0.40		a	g							
1H-1, 75	0.75		r	m							
1H-1, 120	1.20		vr	—							
1H-CC, 15-16	7.64	7.65	vr	—		b	b	vr	b	Y	late Pleist.
2H-CC, 37-38	17.75	17.76	b	—		b	b	b	b		
3H-CC, 37-38	27.27	27.27	b	—		b	b	b	b		
4H-CC, 21-22	36.29	36.30	b	—		b	b	r	b		
5H-CC, 37-38	54.12	54.13	b	—		b	b	b	b		
6H-CC, 55-56	55.83	55.84	b	—		b	b	b	b		
7H-CC, 82-83	64.20	64.21	b	—		b	b	b	b		
8H-CC, 43-44	74.17	74.18	b	—		b	b	b	b		
9H-4, 67	79.17		b	—		b	b	b	b		
9H-4, 68	79.18		r	—							
9H-CC, 75-76	84.24	84.25	vr	—		b	b	r	b		
10X-CC, 45-46	88.45	88.46	tr	—		b	b	vr	b		
11X-CC, 47-48	102.75	102.76	tr	—		b	b	vr	b		
12X-CC, 26-27	110.98	110.99	b	—		b	b	vr	b		
13X-CC, 21-22	120.53	120.54	vr	—		b	b	b	b		
14X-CC, 18-19	130.85	130.86	tr	—		b	b	vr	b		
15X-2, 37		133.67	r	—		b	b	b	b		
15X-2, 139		134.69	r	—							
15X-CC, 10-11	138.39	138.40	tr	—		b	b	vr	b		
16X-CC, 11-12	145.72	145.73	b	—		b	b	b	b		
17X-CC, 22-23	159.75	159.76	b	—		b	b	b	b		
18X-CC, 8-9	164.19	164.20	b	—		b	b	vr	b		
19X-CC, 10-11	180.19	180.20	b	—		b	b	b	b		

occur in Unit II (937B-3H-CC, 28-37 cm [27 mbsf], and 937B-8H-CC, 34-43 cm [74 mbsf]). The occurrence of both iron-stained planktonic foraminifers and pteropods in Sample 937B-8H-CC, 34-43 cm (74 mbsf), suggests that reworked and pelagic components are mixed at this site.

Benthic Foraminifers

Benthic foraminifers are rare or absent in Hole 937B. Rare deep-water, low-oxygen, abyssal benthic foraminifers (*Pyrgo* spp.) are found in Subunits IIB and IIC.

Siliceous Microfossils

Site 937 is barren of diatoms except for the mud-line sample (Table 4). The diatom assemblage consists of rare marine forms as well as a freshwater species (*Melosira granulata*). Siliceous sponge spicules are present in low abundances throughout Hole 937B.

Palynology

Eight samples were examined from Hole 937B (Table 5). In general, they have low abundances and moderate preservation. Two samples at 0.34 mbsf and 0.39 mbsf (Samples 937B-1H-1, 34-36 cm, and -1H-1, 39-41 cm) from the Holocene (Z Zone) have very low abundance and poor preservation with only monolet spores present. A third sample from 7.64 mbsf (Sample 937B-1H-CC, 15-16 cm), within the clays of Unit II, has a relatively greater pollen and spore abundance and is moderately well-preserved. The assemblage includes *Mabea* pollen and monolet spores and is similar to the abundant and well-preserved late Pleistocene (Y Zone) assemblages obtained from other sites (e.g., Table 5 of "Site 936" chapter, "Biostratigraphy" section, this volume). The late Pleistocene (Y Zone) pollen and spore assemblage has low to moderate abundance with Compositae, monosulcate (probably *Palmae*), tricolporate (TCP), and triplicate (TP) pollen types. Cyatheaceae and monolet spores are also present. Dinoflagellates were not found. Wood particles were

observed in all microscope slides in varying abundance. Macroscopic (>63 μ m) organic material was observed in Pleistocene core-catcher samples between 138.30 mbsf and 180.10 mbsf.

Stratigraphic Summary

Unit I contains nannofossil and planktonic foraminifer assemblages indicative of the Holocene. The nannofossil assemblages are well preserved and represent nannofossil Zone CN15b. Unit I is barren of pollen and spores, which is characteristic of the Holocene (Z Zone) calcareous clay at most Leg 155 sites. The Ericson Z/Y boundary is poorly constrained by core-catcher foraminifer samples. It is most likely located near the base of Unit I, given the downhole contamination of core-catcher samples. Planktonic foraminifers are found in moderate abundance in Unit II, whereas nannofossils occur in low abundance or are absent. All of Unit II below the Z/Y boundary has been defined as the Y zone on the basis of the absence of *G. menardii* and *G. tumida*. The age of this unit can also be constrained to younger than 40 ka due to the absence of *P. obliquiloculata*.

PALEOMAGNETISM

Remanence Studies

Archive-half sections from 18 of the 20 APC cores were measured on the pass-through cryogenic magnetometer. Only heavily disturbed Cores 937A-1H and 937B-7H were not measured. Archive-half sections from all 10 XCB cores drilled in Hole 937B were also measured.

The Tensor tool was run using conventional batteries on Cores 937B-3H through -9H, but failed on the last core. For Cores 937C-3H through -8H, nickel-cadmium batteries were used, and the tool appeared to perform well on all cores. Except for Core 937C-5H, the corrected declinations were centered near 0°. Agreement between holes was particularly good below 47 mbsf, although these lower APC cores displayed considerable declination change, or twisting, within each core (Fig. 15).

Table 4. Foraminifer abundance data for Hole 937B.

Core, section, interval (cm)	Top interval (mbsf)	Bottom interval (mbsf)	<i>Globorotalia menardii</i>	<i>Globorotalia tumida</i>	<i>Globorotalia tumida flexuosa</i>	<i>Pulleniatina obliquiloculata</i>	<i>Globigerinoides ruber</i> (white)	<i>Globigerinoides ruber</i> (pink)	<i>Globorotalia hexagonus</i>	<i>Neogloboquadrina dutertrei</i>	<i>Globorotalia trilobus trilobus</i>	<i>Globorotalia inflata</i>	<i>Globorotalia truncatulinoides</i>	<i>Globigerina bulloides</i>	<i>Globigerinoides trilobus sacculifer</i>	<i>Globorotalia fimbriata</i>	<i>Bolliella adamsi</i>	<i>Hastigerinella digitata</i>	<i>Globigerina calida calida</i>	<i>Globorotalia crassaformis hessi</i>	<i>Globorotalia crassaformis viola</i>	<i>Globorotalia tosaensis</i>	<i>Globorotalia crassaformis crassaformis</i>	Others	Vivamite nodules	Overall foraminifer abundance	Preservation	Abundance of bathyal benthic foraminifers	Abundance of abyssal benthic foraminifers	Comments	Ericson Zone	Age			
155-937B-																																			
1H-CC, 6-15	7.55	7.64	R	F	B	B	C	R	B	C	C	B	B	B	F	R	B	B	B	B	B	B	B	R	F	R	G	B	R	SF	Z?	Holocene?			
2H-CC, 28-37	17.66	17.75	R	R	B	F	F	R	B	C	F	B	F	B	F	B	B	B	B	B	B	B	B	A	R	G	B	R	SP	Y	late Pleist.				
3H-CC, 28-37	27.17	27.26	B	B	B	B	C	R	B	C	C	B	C	B	F	B	B	B	B	B	B	B	B	A	C	M	B	R	IS, SP	Y	late Pleist.				
4H-CC, 12-21	36.20	36.29	B	B	B	B	C	B	B	C	C	B	C	B	C	B	B	B	B	B	B	B	B	C	F	G	B	R	Y	Y	late Pleist.				
5H-CC, 28-37	54.03	54.12	B	B	B	B	C	R	B	C	F	B	B	B	C	B	B	B	B	B	B	B	B	F	F	G	B	R	M	Y	late Pleist.				
6H-CC, 46-55	55.74	55.83	B	B	B	B	F	B	B	C	C	B	F	B	C	B	B	B	B	B	B	B	B	A	R	G	B	B	SP	Y	late Pleist.				
7H-CC, 73-82	64.11	64.20	B	B	B	B	F	B	B	C	F	B	C	B	C	B	B	B	B	B	B	B	B	C	F	G	B	B	SP	Y	late Pleist.				
8H-CC, 34-43	74.08	74.17	B	B	B	B	B	B	B	B	B	B	B	B	B	B	B	B	B	B	B	B	B	A	F	G	B	B	PT, IS	Y	late Pleist.				
9H-CC, 67-75	84.15	84.24	B	B	B	B	F	B	B	C	C	B	C	B	C	B	B	B	B	B	B	B	B	A	B	M	B	B	Y	Y	late Pleist.				
10X-CC, 36-45	88.36	88.45	B	B	B	B	R	B	B	A	B	B	C	B	C	B	B	B	B	B	B	B	B	R	A	F	G	B	B	PT	Y	late Pleist.			
11X-CC, 38-47	102.66	102.75	B	B	B	B	F	B	B	C	C	B	F	B	C	B	B	B	B	B	B	B	B	A	R	G	B	B	PT	Y	late Pleist.				
12X-CC, 17-26	110.89	110.98	B	B	B	B	F	B	B	C	C	B	F	B	C	B	B	B	B	B	B	B	B	A	F	G	B	R	Y	Y	late Pleist.				
13X-CC, 12-21	120.44	120.53	B	B	B	B	F	B	B	A	F	B	A	B	R	B	B	B	B	B	B	B	B	A	F	G	B	B	Y	Y	late Pleist.				
14X-CC, 9-18	130.76	130.85	B	B	B	B	F	B	B	A	F	B	A	B	R	B	B	B	B	B	B	B	B	C	R	G	B	B	PT	Y	late Pleist.				
15X-CC, 1-10	138.30	138.39	B	B	B	B	F	R	B	F	R	B	F	B	R	B	B	B	B	B	B	B	B	F	F	M	R	B	AM	Y	late Pleist.				
16X-CC, 2-11	145.63	145.72	B	B	B	B	F	B	B	F	R	B	F	B	R	B	B	B	B	B	B	B	B	C	F	M	B	B	AM	Y	late Pleist.				
17X-CC, 13-22	159.66	159.75	B	B	B	B	R	B	B	F	F	B	F	B	R	B	B	B	B	B	B	B	B	F	F	M	B	B	PT	Y	late Pleist.				
18X-CC, 0-9	164.11	164.20	B	B	B	B	F	B	B	F	F	B	F	B	F	B	B	B	B	R	B	B	B	F	F	M	B	B	Y	Y	late Pleist.				
19X-CC, 1-10	180.10	180.19	B	B	B	B	R	B	B	R	F	B	B	B	B	B	B	B	B	B	B	B	B	F	R	M	B	B	M, W	Y	late Pleist.				

Notes: Key to Comments section: Sediment composition: PT = pteropods, M = mica, AM = authigenic minerals; indicators of reworking: SF = shell fragments, W = wood fragments, SP = spines, IS = iron-stained foraminifers. Note also the occurrence of bathyal benthic foraminifers.

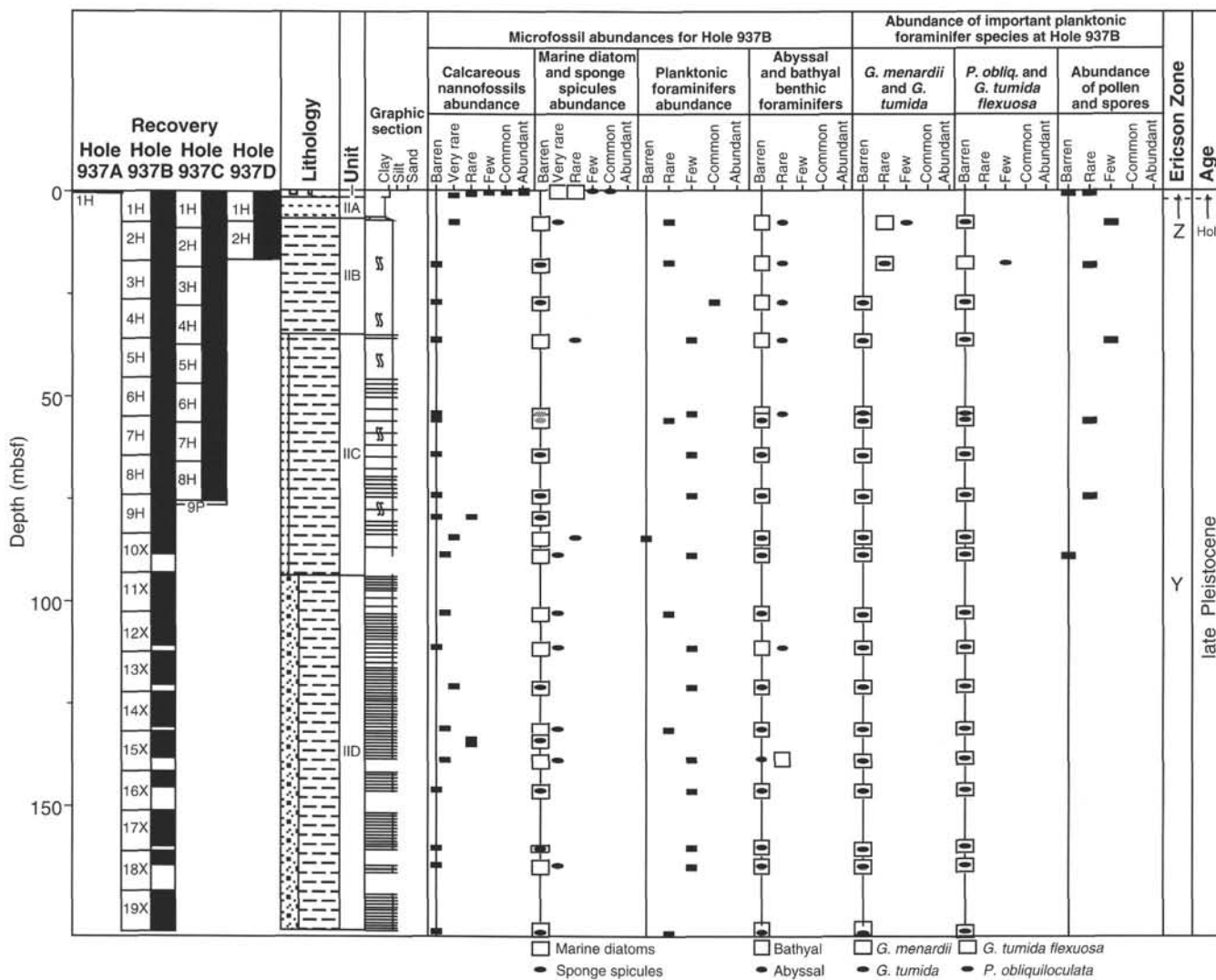


Figure 14. Biostratigraphic summary for Site 937.

Table 5. Spores and pollen data for Hole 937B.

Core, section, interval (cm)	Top interval (mbsf)	Bottom interval (mbsf)	Pollen and spores			Dinocysts	Wood/ carbonized particles	Ericson Zone (inferred from forams.)	Age (inferred from forams.)
			Abundance	Preservation	Major types recorded				
155-937B-									
1H-1, 34-36	0.34	0.36	b			b	r	Z	Holocene
1H-1, 39-41	0.39	0.41	r	p	Monolete (psilate) spore	b	c	Z?	Holocene?
1H-CC, 15-16	7.64	7.65	f	m	<i>Mabea</i> , monolete (psilate) spore	b	a	Z?	Holocene?
2H-CC, 37-38	17.75	17.76	r	m	Monoluscus (Palmae?)	b	f	Y	late Pleist.
4H-CC, 21-22	36.29	36.30	f	p	TP, TCP	b	c	Y	late Pleist.
6H-CC, 55-56	55.83	55.84	r	m	Cyatheaceae	b	f	Y	late Pleist.
8H-CC, 43-44	74.17	74.18	r	m	Compositae	b	c	Y	late Pleist.
10X-CC, 45-46	88.45	88.46	b			b	f	Y	late Pleist.

Notes: TCP = tricolporate; TP = triporate.

Inclinations at this site follow the pattern established in previous sites. In the APC cores, they are centered on 0° after AF demagnetization, but in the XCB cores (>83.5 mbsf) they are nearly always >0°. The intensity of remanence shows a pronounced increase in the interval from 63 to 83 mbsf (Fig. 16). These depths correspond to a zone of closely spaced silt laminae (Fig. 5).

Figure 17 shows an extended interval of apparent secular variation in inclination (Cores 937B-1H through -5H). In Hole 937B, 34 cycles are observed in the depth interval of 1 to 45 mbsf.

No geomagnetic excursions were identified in the cores measured from this site.

Magnetic Susceptibility

Whole-core magnetic susceptibility was measured on all cores from Site 937, except for Core 937A-1H. Discrete-sample measurements were performed on Hole 937B. The whole-core data from Hole 937B are used to represent the site in Figure 18.

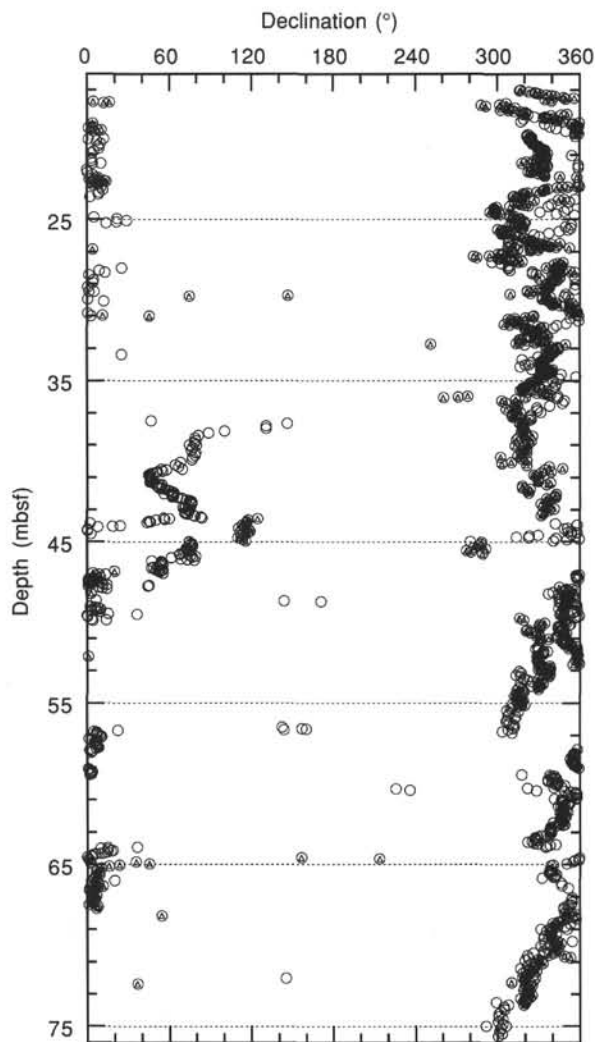


Figure 15. Azimuthally corrected declinations for APC cores from Holes 937B (open circles) and 937C (open triangles), after AF demagnetization to 20 mT.

The highest whole-core values are within Subunit IIC, and the lowest values occur in Unit I and near the bottom of Subunit IID. The highest discrete-sample values (65 and 80 mbsf) correspond to a high magnetic remanence intensity zone (Fig. 16). The susceptibility data do not show sharp changes across unit or subunit boundaries.

ORGANIC GEOCHEMISTRY

Volatile Hydrocarbons

Headspace methane concentrations increase rapidly below the sediment surface to a maximum value of 25,150 ppm at 13.50 mbsf (Table 6; Fig. 19). Methane concentrations remain fairly constant below this depth, ranging from 6,600 ppm to 15,000 ppm. Vacutainer methane values range from 75,000 ppm at 13.50 mbsf to 793,000 ppm at 43.50 mbsf. Higher molecular weight hydrocarbons were not detected, indicating a predominantly biogenic methane source at Site 937.

Carbon, Nitrogen, and Sulfur Concentrations

High carbonate contents, calculated as CaCO_3 , are found at 0.02 mbsf (48%), 0.32 mbsf (21%), and 0.48 mbsf (8%). The rest of Hole

937B has low carbonate concentrations (0.6% to 3.7%) except for the sample at 154.63 mbsf, which has 24% carbonate (Table 7; Fig. 20) and corresponds to a light-colored clast. TOC is less than 0.5% in the top three samples and increases downhole to 0.9% at 6.55 mbsf. Most TOC values in the rest of the hole range from 0.8% to 1%, except for low concentrations (0.5% to 0.7%) measured in silt and sand layers.

Total nitrogen concentrations are low ($\leq 0.05\%$) in the top 0.48 mbsf, increasing to 0.09% at 10.63 mbsf. Below this depth, most TN concentrations in Hole 937B range from 0.08% to 0.14%. They generally display a downhole profile similar to TOC, with lower concentrations (TN $\leq 0.08\%$) in silt and sand beds (Fig. 20). Total sulfur concentrations, which range between 0% and 0.07% in most of Hole 937B, are relatively high in the interval between 3.47 mbsf and 10.63 mbsf (maximum value of 1.4% at 8.80 mbsf).

The high carbonate content and low TOC and TN observed in the top 0.5 mbsf are characteristic of Holocene sediment (Unit I) throughout previous Leg 155 sites. Also similar to conditions at previous sites are the high sulfur values observed below the carbonate-rich Unit I in Subunit IIA. Below the TS maximum at 8.80 mbsf, the elemental composition of the sediment is fairly uniform. The major variations in TOC and TN concentrations are associated with changes in grain size. Most sediment samples in Hole 937B have [C/N] ratios of 8 to 12 (Table 7), with high values of 14 to 16 between 3.47 mbsf and 8.15 mbsf.

INORGANIC GEOCHEMISTRY

Interstitial Water Analysis

Interstitial water samples were collected from nine sediment samples at Hole 937B. Samples were taken approximately every 10 m for the upper 40 mbsf and approximately every 20 to 30 m thereafter to a depth of 157.10 mbsf (Table 8; Fig. 21).

Salinities of the water samples range from 32.0 to 34.0 (Fig. 21A). In the upper 25.95 m of the hole, salinity decreases from 34.0 to 32.0. From 30.95 to 69.22 mbsf salinity increases to 33.5, and then decreases again to 32.0 at 157.10 mbsf.

Chloride concentrations increase from 550 to 557 mM between 1.45 and 25.95 mbsf (Fig. 21B), and are relatively constant thereafter, varying between 557 and 561 mM.

Pore-water pH decreases from 7.77 at 1.45 mbsf to 7.24 at 25.95 mbsf (Fig. 21C). The values then increase downhole to 7.58 at 69.22 mbsf, and maintain a value of around 7.5 to near the bottom of the hole.

Alkalinity varies from 6.95 to 14.02 mM (Fig. 21D). For the interval from 1.45 to 13.45 mbsf, alkalinity is around 13 mM. The values decrease to between 6.95 and 8.42 mM from 25.95 to 51.45 mbsf. Below 51.45 mbsf, the values increase again to between 11.37 and 14.02 mM for the remainder of the hole.

Magnesium and calcium profiles are similar to those at all previous sites. The concentrations are 47.6 mM magnesium and 8.1 mM calcium at 1.45 mbsf. They decrease further, to around 41 and 5 mM, respectively, by 13.45 mbsf (Fig. 21E and 21F), and are fairly constant below that depth.

Pore-water sulfate concentrations decrease from seawater values to 14.1 mM at 1.45 mbsf and to zero by 13.45 mbsf (Fig. 21G). The values remain at or near zero for the remainder of the hole.

Ammonium concentrations increase with depth over the entire hole, though more slowly with increasing depth (Fig. 21H). Ammonium concentration is 0.5 mM at 1.45 mbsf and increases to 9.7 mM near the bottom of the hole.

Pore-water phosphate concentrations are at a maximum of 99.1 μM at 1.45 mbsf (Fig. 21I). The phosphate concentrations decrease to 7.9 μM at 13.45 mbsf, and generally remain below 10 μM for the remainder of the hole.

Dissolved silica concentrations increase from 275 μM at 1.45 mbsf to 502 μM at 69.22 mbsf (Fig. 21J). Thereafter, values decrease slightly to between 429 and 449 μM downhole.

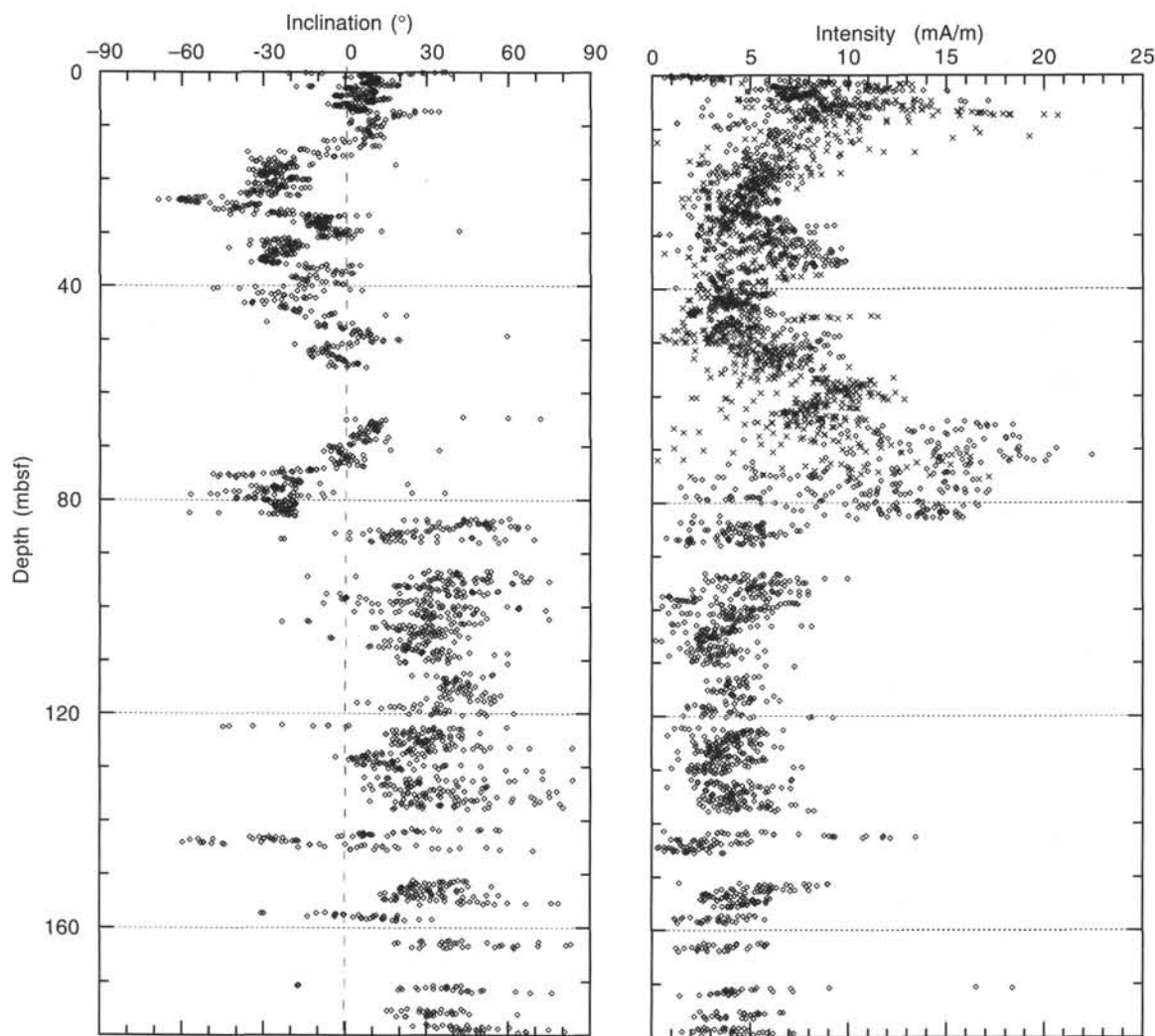


Figure 16. Inclinations and intensity of archive-half sections from Holes 937B (diamonds) and 937C (x's), after AF demagnetization to 20 mT.

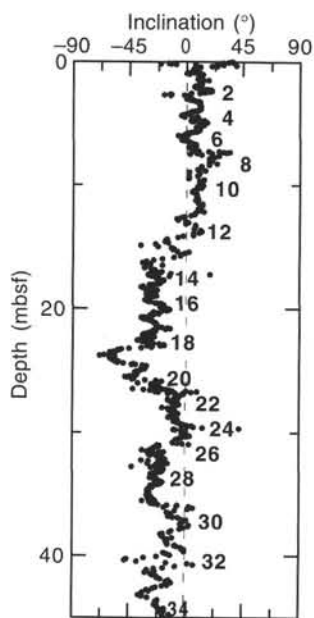


Figure 17. Secular variation in inclination for the first 45 m in Hole 937B. Even-numbered cycles are indicated.

Pore-water potassium concentrations decrease from 11.8 mM at 1.45 mbsf to 7.1 mM at 69.22 mbsf (Fig. 21K). From 69.22 mbsf to near the bottom of the hole, the values are more constant, varying between 7.1 and 8.0 mM.

Dissolved sodium concentrations decrease from 468 mM at 1.45 mbsf to 455 mM at 30.95 mbsf, then increase again to 464 mM at 69.22 mbsf (Fig. 21L). Below 69.22 mbsf, the values are quite constant, varying from 461 to 463 mM.

Iron concentrations at Hole 937B include the highest concentrations measured on Leg 155. The concentrations increase quickly in the upper 30 m, from 14 μM at 1.45 mbsf to 281 μM at 30.95 mbsf (Fig. 21M), then decrease to 106 μM at 69.22 mbsf. A local maximum of 290 μM is observed at 99.18 mbsf, below which the concentrations decrease to between 21 and 55 μM downhole.

Manganese concentrations are at a maximum of 14.0 μM at 1.45 mbsf (Fig. 21N). The concentrations decrease to 4.0 μM at 51.54 mbsf, and are relatively constant, varying from 3.2 to 6.0 μM , through the remainder of the hole.

Sediment Geochemistry

Two muds were sampled for major- and trace-element geochemistry (Tables 9 and 10) at depths of 71.17 mbsf and 119.00 mbsf. Both muds are from silty intervals of the Yellow Channel-levee System of the Upper Levee Complex. Compositional abundances and alumina-normalized ratios are very similar to those from muds sampled and other Leg 155 sites, with SiO_2 of 61 and 62 wt%, and Al_2O_3 of 21 and

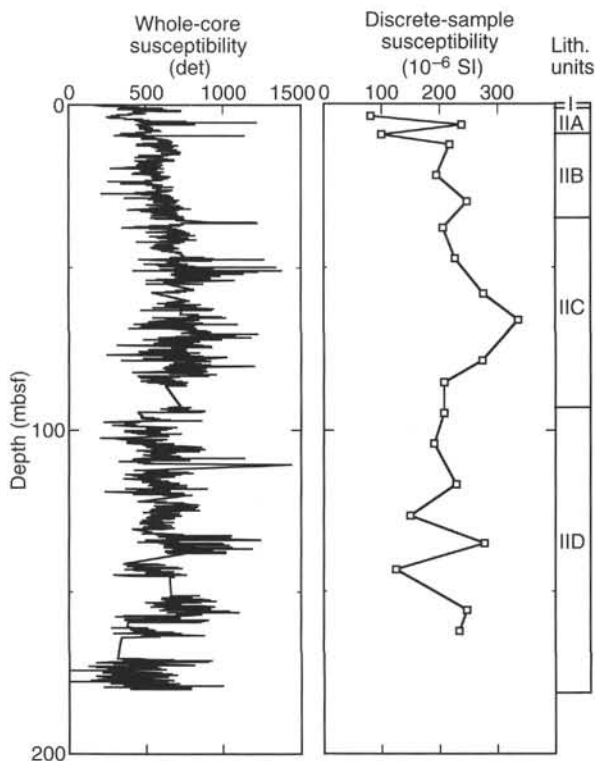


Figure 18. Magnetic susceptibility data and lithostratigraphic units for Hole 937B. Whole-core susceptibility data has been corrected to remove effect of compaction.

Table 6. Gas concentrations in sediments from Site 937.

Core, section, interval (cm)	Depth (mbsf)	Sed. temp.* (°C)	Methane	
			HS (ppm)	VAC (ppm)
155-937B-				
1H-2, 0-5	1.50	2	6	
2H-5, 0-5	13.50	2	15,429	75,342
3H-7, 0-5	26.00	3	9,764	571,188
4H-4, 0-5	31.00	3	8,488	576,817
5H-6, 0-5	43.50	3	9,578	792,833
6H-4, 0-5	49.68	4	9,380	539,741
7H-2, 0-5	55.29	4	9,442	125,427
8H-4, 0-5	67.82	4	8,971	105,223
9H-6, 0-5	81.50	5	8017	557,253
10X-3, 0-5	86.50	5	8,160	
11X-6, 0-5	99.28	5	8,507	119,185
12X-5, 0-5	108.70	5	8,725	
13X-5, 0-5	118.40	6	15,218	
14X-5, 0-5	128.10	6	13,211	
15X-3, 0-5	134.80	6	7,541	
16X-3, 0-5	144.50	7	13,634	
17X-5, 0-5	157.20	7	6,570	
18X-2, 0-5	162.40	7	8,345	97,600

Notes: HS = headspace; VAC = vacutainer. Geothermal gradient = 32°C/km. Bottom-water temperature = 2°C. *See "In-situ Temperature Measurements" section, this chapter.

22 wt%. A minor carbonate component may contribute to slightly elevated abundances of CaO (0.9 and 1.1 wt%).

PHYSICAL PROPERTIES

Index Properties

Index properties were determined for all lithologic units in Hole 937B (Table 11). Water content decreases uniformly with depth from 54% in the foraminifer-nannofossil clay of Unit I to 25% in silty clay

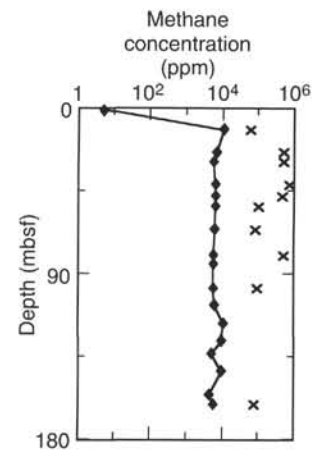


Figure 19. Methane concentrations at Site 937. Headspace (diamond) and vacutainer (x) samples are plotted.

at the base of Hole 937B (Fig. 22). Over this interval, the corresponding decrease in porosity is from 76% to 46%. Water content changes most rapidly in the uppermost part of Unit II with values decreasing from 50% at 2.02 mbsf to 39% at 9.60 mbsf. In the lower part of Hole 937B, several cores (Cores 937B-16X, -18X, and -19X; Table 11) display distinct 1% to 3% decreases in water content over the length of each core. This pattern has been observed at previous Amazon Fan sites, most notably Site 932, and has been attributed to sediment expansion in the core barrel during coring.

Grain density in Hole 937B averages 2.74 g/cm³ with most of the values ranging from 2.7 to 2.8 g/cm³ (Table 11). Because of the low variability of grain density, downhole variation of wet-bulk density essentially matches the variation in water content (Fig. 22). From near the seafloor to the base of Hole 937B, wet-bulk density increases from approximately 1.5 to 2.0 g/cm³. Comparison of the discrete-sample wet-bulk densities with the GRAPE bulk density profile provides a measure of the expansion experienced by the cores. The two data sets diverge at about 3.5 mbsf (Fig. 22). Below this depth the GRAPE densities are approximately 0.2 to 0.4 g/cm³ less than the discrete sample values.

Compressional-wave Velocity

Compressional-wave velocity measurements were limited to those made with the PWL. The pervasive microfractures in sediment affected by gas expansion restricted measurements to the interval from 0 to 4.5 mbsf. The average transverse velocities determined by the PWL for cores from Holes 937B, 937C, and 937D are 1495, 1476, and 1492 m/s, respectively.

Shear Strength

Measurements of undrained shear strength were made using the motorized shear vane on all cores from Hole 937B (Table 12). Below 36 mbsf, compressive strengths were determined using a pocket penetrometer. The correlation between shear-strength values estimated from the compressive strength and those determined by the lab vane is good ($r = 0.88$); however, the regression equation ($S_{u[est]} = 0.75 \cdot q_u/2 + 5.9$) indicates that the penetrometer yields measurements that overestimate the lab vane values.

The strength profile for Hole 937B can be divided into two parts at approximately 84 mbsf (Fig. 23). This depth corresponds to the change from APC to XCB coring. Within the upper interval, undrained shear strength increases relatively uniformly from 6.9 kPa just below the seafloor to 48.9 kPa at 83.24 mbsf. This trend is interrupted by a local maximum of 27.9 kPa at 33.11 mbsf. This maximum occurs independent of water content or bulk density changes.

Table 7. Elemental and organic carbon compositions of sediments from Site 937.

Core, section interval (cm)	Depth (mbsf)	IC (%)	CaCO ₃ * (%)	TC (%)	TOC (%)	TN (%)	TS (%)	[C/N]a
155-937B-								
1H-1, 2-3	5.73	0.02	47.7	6.15	0.42	0.04	0.00	11
1H-1, 32-33	0.32	2.47	20.6	2.75	0.28	0.04	0.00	9
1H-1, 48-49	0.48	0.95	7.9	1.42	0.47	0.05	0.03	12
1H-3, 47-48	3.47	0.08	0.7	0.85	0.77	0.06	0.50	16
1H-4, 54-55	5.04	0.07	0.6	0.78	0.71	0.05	0.10	16
1H-5, 55-56	6.55	0.11	0.9	1.03	0.92	0.07	0.17	16
2H-1, 65-66	8.15	0.31	2.6	1.17	0.86	0.07	0.59	14
2H-1, 130-131	8.80	0.16	1.3	0.99	0.83	0.08	1.41	12
2H-3, 13-14	10.63	0.24	2.0	1.12	0.88	0.09	0.13	12
3H-3, 54-55	20.54	0.12	1.0	0.89	0.77	0.09	0.04	11
4H-3, 50-51	30.00	0.16	1.3	0.96	0.80	0.08	0.02	12
4H-6, 50-51	34.50	0.21	1.7	1.19	0.98	0.08	0.00	14
5H-3, 47-48	39.47	0.25	2.1	1.31	1.06	0.11	0.14	11
5H-6, 47-48	43.97	0.25	2.1	1.33	1.08	0.10	0.00	12
6H-3, 61-62	48.79	0.27	2.2	1.22	0.95	0.10	0.05	11
6H-5, 110-111	52.28	0.28	2.3	1.25	0.97	0.10	0.07	11
7H-2, 89-90	56.18	0.30	2.5	1.25	0.95	0.09	0.00	12
7H-6, 138-139	60.26	0.29	2.4	1.23	0.94	0.10	0.00	11
8H-2, 82-83	65.80	0.35	2.9	1.36	1.01	0.11	0.00	11
8H-6, 33-34	71.15	0.26	2.2	1.20	0.94	0.09	0.00	12
9H-1, 57-58	74.57	0.18	1.5	0.81	0.63	0.06	0.07	12
9H-1, 58-59	74.58	0.17	1.4	0.86	0.69	0.07	0.00	12
10X-2, 82-83	85.82	0.28	2.3	1.25	0.97	0.10	0.07	11
10X-3, 108-109	87.58	0.23	1.9	1.12	0.89	0.12	0.06	9
11X-3, 50-51	95.28	0.30	2.5	1.33	1.03	0.14	0.05	9
11X-6, 50-51	99.78	0.29	2.4	1.31	1.02	0.14	0.06	8
12X-3, 63-64	106.33	0.22	1.8	1.29	1.07	0.13	0.07	9
13X-1, 103-104	113.43	0.16	1.3	0.79	0.63	0.09	0.00	8
13X-5, 58-59	118.98	0.45	3.7	1.14	0.69	0.08	0.07	10
14X-2, 119-120	124.79	0.31	2.6	1.32	1.01	0.11	0.04	11
14X-4, 119-120	127.79	0.29	2.4	1.31	1.02	0.13	0.05	9
15X-2, 29-30	133.59	0.20	1.7	0.88	0.68	0.07	0.05	12
15X-2, 35-36	133.65	0.32	2.7	1.34	1.02	0.10	0.00	12
16X-2, 119-120	144.19	0.32	2.7	1.26	0.94	0.11	0.07	10
17X-1, 60-61	151.80	0.34	2.8	1.36	1.02	0.12	0.06	10
17X-3, 43-44	154.63	2.87	23.9	4.15	1.28	0.14	0.03	10
18X-2, 42-43	162.82	0.28	2.3	1.24	0.96	0.11	0.06	10
18X-2, 109-110	163.49	0.21	1.7	0.71	0.50	0.08	0.00	7
19X-5, 39-40	176.99	0.35	2.9	1.45	1.10	0.14	0.05	9

* Calculated assuming all IC is calcite.

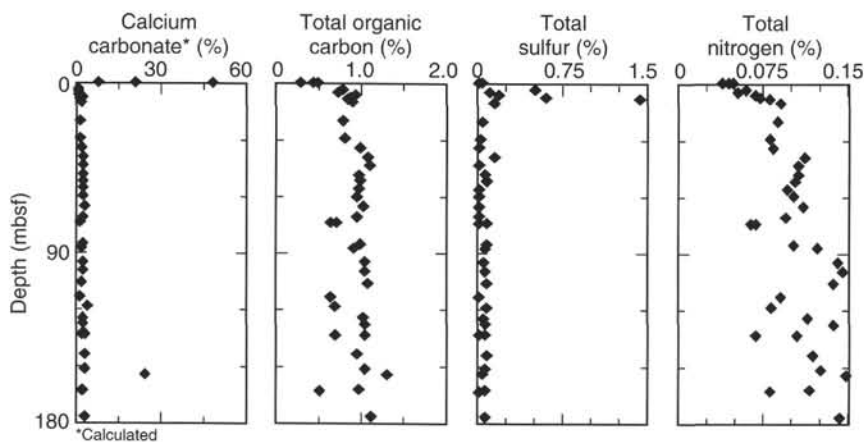


Figure 20. Concentration profiles of calcium carbonate, total organic carbon, total sulfur, and total nitrogen in Hole 937B.

Below 84 mbsf, strength values continue to increase with depth, but with greater variability. The lab vane and compressive-strength values for the shear strength at the base of Hole 937B are 64.3 and 88.2 kPa, respectively.

A prominent feature of the lower part of the strength profile is the pattern of strength increasing with depth within individual cores. This pattern is well developed in Cores 937B-14X through -19X. The strength increases are associated with decreasing water content in Cores 937B-16X, -18X, and -19X; however, the changes in shear strength are noticeably greater in magnitude than the water content changes. As with the index properties, the changes in shear and compressive strengths have been attributed to expansion of the upper part and compression of the lower part of cores during coring.

The residual undrained shear strength also increases with depth in Hole 937B (Table 12), but at a lower rate than the peak strength. The

result is a slight downhole decrease in the ratio of residual to peak undrained shear strength (Fig. 23). In Cores 937B-14X through -19X, decreases in the ratio of residual to peak strength roughly match the downcore increases in peak strength. Changes in the ratio that are a function of peak strength variation indicate that disturbance during coring is responsible for peak strength change, and not lithologic or bulk property differences, because residual strength is not significantly affected by disturbance.

Resistivity

Longitudinal and transverse resistivity were determined for Hole 937B (Table 13). Longitudinal resistivity displays a general downhole increase that parallels the downhole decrease in porosity. Resistivity increases from 0.26 Ω m near the seafloor to 0.44 Ω m at the

Table 8. Interstitial water chemistry, Site 937.

Core, section, interval (cm)	Depth (mbsf)	Salinity	pH	Alkalinity (mM)	Cl ⁻ (mM)	Mg ²⁺ (mM)	Ca ²⁺ (mM)	K ⁺ (mM)	HPO ₄ ²⁻ (μM)	SO ₄ ²⁻ (mM)	NH ₄ ⁺ (mM)	H ₄ SiO ₄ (μM)	Na ⁺ (mM)	Fe ²⁺ (μM)	Mn ²⁺ (μM)
155-937B-															
1H-1, 145-150	1.45	34.0	7.77	12.71	550	47.6	8.1	11.8	99.1	14.1	0.5	275	468	14	14.0
2H-4, 145-150	13.45	33.0	7.51	13.62	556	41.0	5.8	10.2	7.9	0.0	3.7	349	462	104	8.8
3H-6, 145-150	25.95	32.0	7.24	6.95	557	41.3	5.3	9.6	2.7	0.0	4.7	255	456	275	7.2
4H-3, 145-150	30.95	32.0	7.26	7.02	557	42.1	5.0	9.1	4.8	0.0	5.9	322	455	281	6.8
5H-5, 145-150	51.45	32.5	7.45	8.42	557	41.1	4.3	8.5	6.7	0.0	6.9	328	460	124	4.0
8H-4, 140-150	69.22	33.5	7.58	12.78	561	42.3	4.6	7.1	8.8	0.0	8.1	502	464	106	4.4
11X-5, 140-150	99.18	33.0	7.55	11.37	559	41.6	4.8	7.9	2.4	0.4	8.2	429	462	290	6.0
14X-4, 140-150	128.00	33.0	7.51	13.12	557	41.9	4.7	7.3	4.0	0.0	9.0	449	461	21	3.2
17X-4, 140-150	157.10	32.0	7.58	14.02	559	41.5	4.5	8.0	11.7	0.3	9.7	436	464	55	3.2

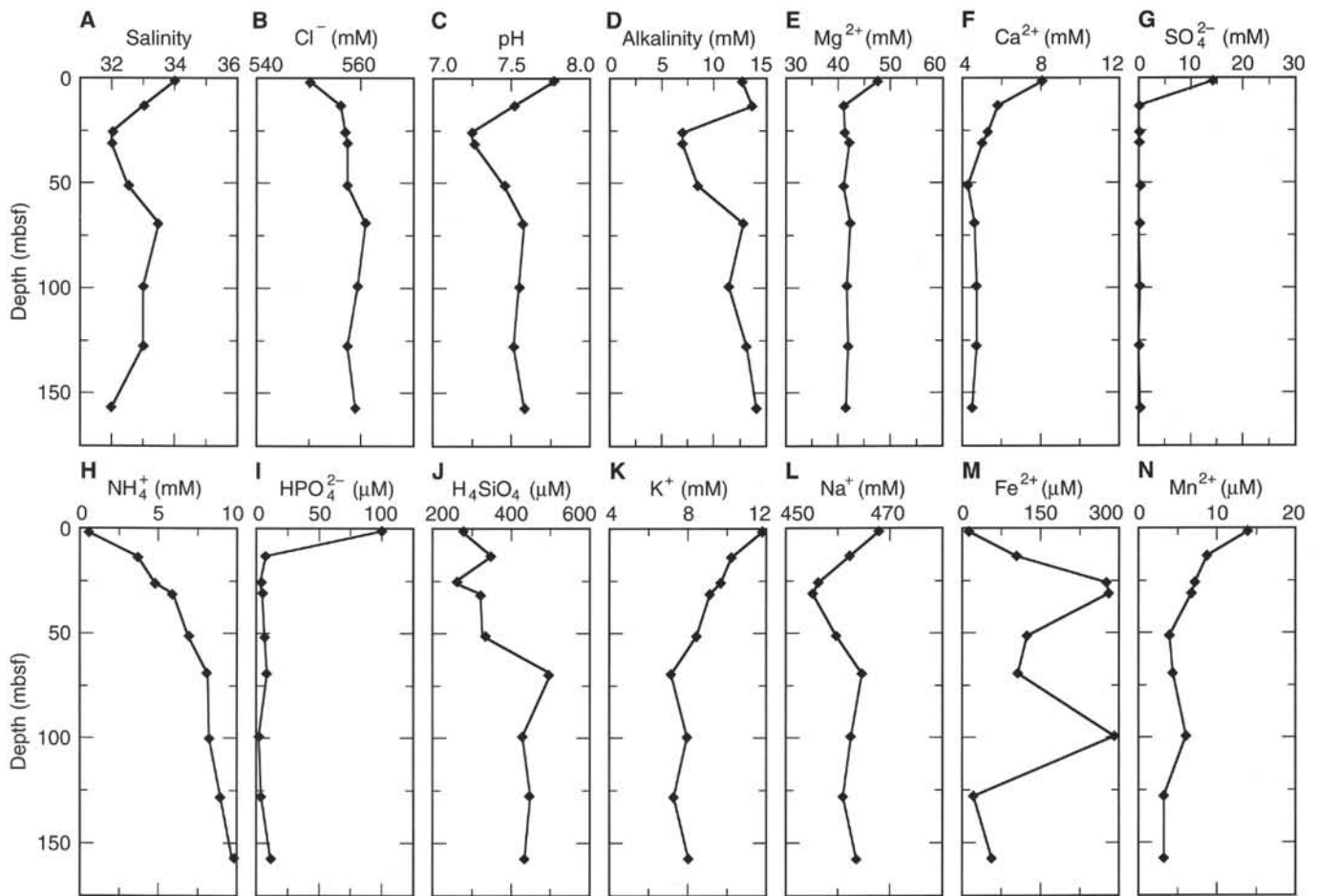


Figure 21. Downcore variation in pore-water chemistry: A. Salinity. B. Chloride. C. pH. D. Alkalinity. E. Magnesium. F. Calcium. G. Sulfate. H. Ammonium. I. Phosphate. J. Silica. K. Potassium. L. Sodium. M. Iron. N. Manganese.

base of Hole 937B. Comparison of longitudinal and transverse resistivities indicates no clear lithologic or downhole trends in resistivity anisotropy (Fig. 24). The anisotropy averages -1% over the length of the hole.

IN-SITU TEMPERATURE MEASUREMENTS

Temperature gradients and heat flow were determined using two downhole measurements and the bottom-water (mud-line) temperature. Two ADARA measurements were made during Cores 937B-6H (55.0 mbsf) and -9H (83.5 mbsf) using instrument number 12. The mud-line temperature of 2.79°C measured from this instrument was used as the reference bottom-seawater temperature at Site 937. Suc-

cessful measurements resulted in extrapolated equilibrium temperatures of 4.65°C at 55 mbsf and 5.37°C at 83.5 mbsf.

Equilibrium temperatures, extrapolated from synthetic curves constructed to fit transient temperature data, are plotted as a function of depth (mbsf) in Figure 25. Using the ADARA mud-line temperature and the sub-bottom temperatures from the two ADARA measurements downhole, the geothermal temperature gradient can be approximated by a linear mean of 31.3°C/km. We calculated heat flow by adopting the constant geothermal temperature gradient of 31.3°C/km and a linear increase in thermal conductivity, K, of 1.1 ± 0.15 W/(m-K), which is an average of regression estimates at 80 mbsf. The calculated heat flow is 34.46 mW/m².

Depending on which data points are used, different estimates can be made of the geothermal gradient. Using the ADARA mud-line

Table 9. Major element composition (wt%) of sediment samples, Site 937.

Core, section, interval (cm)	Depth (mbsf)	Lithology	SiO ₂	TiO ₂	Al ₂ O ₃	Fe ₂ O ₃	MnO	MgO	CaO	Na ₂ O	K ₂ O	P ₂ O ₅	Total	LOI
155-937B-8H-6, 35-40	71.17	Mud	62.25	1.05	20.64	7.81	0.12	2.13	1.09	1.62	2.86	0.20	99.77	7.96
13X-5, 60-65	119.00	Mud	61.21	1.08	21.78	8.14	0.12	2.20	0.94	1.60	2.94	0.19	100.19	8.42

Notes: Total iron is reported as Fe₂O₃. LOI = loss on ignition.

Table 10. Trace element composition (ppm) of sediment samples, Site 937.

Core, section, interval (cm)	Depth (mbsf)	Lithology	Ba	Ce	Cr	Cu	Nb	Ni	Rb	Sr	V	Y	Zn	Zr
155-937B-8H-6, 35-40	71.17	Mud	508	98	67	33	22	33	123	178	88	39	123	242
13X-5, 60-65	119.00	Mud	513	109	67	33	21	35	128	160	90	39	127	224

temperature and the one ADARA measurement at 55.0 mbsf, the geothermal gradient is 33.8°C/km (Fig. 25). If we use only both ADARA temperatures (Fig. 25), the geothermal gradient is 25.3°C/km.

SYNTHESIS AND SIGNIFICANCE

Stratigraphic Synthesis

Surficial Nannofossil-foraminifer Clay (Unit I)

Unit I (0–0.85 mbsf) is an intensely bioturbated Holocene nannofossil-foraminifer clay (Fig. 26), with about 48% carbonate at the top of the unit decreasing to 8% near the base. The unit includes four indurated iron-rich clay crusts between 0.15 and 0.38 mbsf.

Bioturbated Mud Equivalent to the Amazon, Aqua, Purple, and Blue Channel-levee Systems (Subunits IIA and IIB)

Subunits IIA (0.85–10.50 mbsf) and IIB (10.49–37.43 mbsf) comprise moderately to intensely bioturbated mud that in Subunit IIB is strongly mottled containing hydrotroilite. At the base of Subunit IIA is a 2.3-m-thick mud with particularly intense black coloration from hydrotroilite (>1% total sulfur) with steeply dipping boundaries, possibly corresponding to diagenetic activity along a fault. Steeply dipping faults have been noted at a number of sites (e.g., 933A-6H-2; 938A-8H-1), but none appear large enough to be visible on 3.5-kHz profiles. Rare pale-blue vivianite patches are present in Subunit IIB. Total organic carbon content is almost constant at 1% from 20 mbsf to the base of the hole. Total sulfur exceeds 0.5% between 3.5 and 11 mbsf.

Subunits IIA and IIB are interpreted to be equivalent to the time when the Amazon, Aqua, and Purple channels were active more than 25 km away from the site and the Blue Channel was active 10 km from the site.

Levee Crest of the Yellow Channel-levee System (Subunits IIC and IID)

The crest of the Yellow levee consists overall of a generally fining-upward sequence similar to that formed at the crest of the Amazon levee. Subunit IIC (37.43–93.51 mbsf) consists of faintly mottled mud with a few laminae and thin beds of silt. The frequency and thickness of silt laminae and beds vary on a scale of a few meters. Large burrows, 1–2 cm in diameter, are particularly obvious along the tops of silt beds and are probably formed by echinoids, whose spines are a common component of the sediment. Subunit IID (93.51–180.3 mbsf) consists of faintly mottled mud with laminae and

thin beds of silt and fine sand. Sand beds are up to 10 cm thick and some are cross laminated.

Implications

Variation in magnetic declination, interpreted as secular variation, is well-developed between 1 and 45 mbsf, corresponding to the interval of the Amazon, Aqua, Purple, and Blue Channel-levee systems. Thirty-four cycles were detected, with wavelength increasing downhole. Although no magnetic excursion was detected at this site, at Sites 931 and 933 the Lake Mungo magnetic excursion (30 ka) is detected below the Blue seismostratigraphic interval, within the Yellow interval. Based on overall sediment thicknesses, we estimate that the age of the top of the Yellow interval is probably in the range of 25–28 ka. This implies that the interval from the base of Unit I (10 ka) to 45 mbsf is of 15–18 k.y. duration, so that the cycles are of average 500 yr duration, similar to those inferred from archeological and observatory data. The downhole increase in wavelength probably indicates that sedimentation rate increases downcore. A higher sedimentation rate is to be expected in the Blue interval, because of the proximity of the Blue Channel.

Calcareous nannofossils are rare or absent in Unit II. Unit II can be constrained in age to less than 40 ka by the absence of *P. obliquiloculata*. Foraminifer abundances are generally moderate in Subunits IIA and IIB, and should be quite sufficient to provide an isotopic and Carbon-14 chronology to be correlated with the secular variation. Foraminifer abundances are low in Subunits IIC and IID. Aragonitic pteropods are found throughout Unit II. Wood fragments are abundant in the lower part of Unit IID.

The total thickness of the Yellow levee is unclear from seismic reflection data, but could be as great as 450 m. As noted at other sites, there is considerable variation in the abundance of silt and sand beds in the levee sections. We were undecided as to whether asymmetric cycles in the frequency of these beds could be distinguished, or whether the beds tended to occur in clusters or packets. This distribution may indicate a source influence on turbidite sedimentation that is perhaps related to climatic or sea-level fluctuations or autocyclic changes in river-mouth sedimentation. The correlative section of the Yellow levee in Site 933 on the middle fan also shows fluctuations in the abundance of silt laminae. Any detailed correlation will require data on the chronology of the two sites.

Clasts of nannofossil-rich clay, typically less than 1 cm in size, occur at several depths in the core. These have acted as nuclei for the precipitation of siderite, which forms loosely cemented nodules. Nannofossils tend to show secondary overgrowths in these clasts. One clast was large enough for larger microfossils to be identified. These included abundant pteropods and warm-water foraminifers,

Table 11. Index properties at Site 937.

Core, section, interval (cm)	Depth (mbsf)	Water content (%)	Wet-bulk density (g/cm ³)	Grain density (g/cm ³)	Dry-bulk density (g/cm ³)	Porosity (%)	Void ratio
155-937B-							
1H-1, 52-54	0.52	53.8	1.47	2.81	0.68	76.1	3.19
1H-2, 52-54	2.02	50.1	1.51	2.70	0.75	72.5	2.64
1H-3, 53-55	3.53	47.6	1.54	2.69	0.81	70.4	2.38
1H-4, 39-41	4.89	46.5	1.59	2.83	0.85	70.6	2.40
1H-5, 75-77	6.75	44.8	1.58	2.67	0.87	67.9	2.12
2H-1, 60-62	8.10	41.8	1.61	2.69	0.94	65.4	1.89
2H-2, 60-62	9.60	39.0	1.70	2.78	1.04	63.4	1.74
2H-3, 55-57	11.05	40.2	1.67	2.69	1.00	63.9	1.77
2H-4, 69-71	12.69	38.3	1.71	2.68	1.05	61.9	1.62
2H-5, 100-102	14.50	38.4	1.74	2.79	1.07	62.9	1.70
2H-6, 32-34	15.32	39.3	1.69	2.77	1.02	63.6	1.75
2H-7, 30-32	16.80	39.5	1.65	2.74	1.00	63.5	1.74
3H-1, 24-26	17.24	37.2	1.72	2.69	1.08	60.8	1.55
3H-2, 42-44	18.92	37.2	1.73	2.71	1.09	61.0	1.57
3H-3, 116-118	21.16	36.4	1.77	2.74	1.12	60.5	1.53
3H-4, 57-59	22.07	36.1	1.74	2.70	1.11	59.8	1.49
3H-5, 30-32	23.30	35.5	1.75	2.69	1.13	59.1	1.44
3H-6, 104-106	25.54	34.4	1.78	2.78	1.17	58.8	1.43
3H-7, 26-28	26.26	35.9	1.77	2.79	1.13	60.4	1.53
4H-1, 38-40	26.88	36.0	1.73	2.74	1.11	60.1	1.51
4H-2, 53-55	28.53	35.6	1.74	2.73	1.12	59.6	1.47
4H-3, 46-48	29.96	34.3	1.73	2.70	1.13	57.9	1.38
4H-4, 52-54	31.52	36.1	1.74	2.72	1.11	60.0	1.50
4H-5, 60-62	33.10	34.0	1.77	2.69	1.17	57.4	1.35
4H-6, 53-55	34.53	33.8	1.78	2.72	1.18	57.5	1.35
5H-1, 71-73	36.71	32.7	1.80	2.70	1.21	56.2	1.28
5H-2, 117-119	38.67	33.3	1.79	2.73	1.20	57.1	1.33
5H-3, 64-66	39.64	33.1	1.66	2.73	1.11	56.9	1.32
5H-4, 95-97	41.45	33.9	1.77	2.71	1.17	57.6	1.36
5H-5, 70-72	42.70	32.6	1.80	2.72	1.21	56.3	1.29
5H-6, 58-60	44.08	33.8	1.64	2.71	1.09	57.5	1.35
5H-7, 58-60	45.58	32.7	1.80	2.71	1.21	56.2	1.28
6H-1, 45-47	45.95	31.6	1.83	2.75	1.25	55.3	1.24
6H-2, 37-39	47.05	32.2	1.82	2.74	1.23	56.0	1.27
6H-3, 49-51	48.67	32.0	1.82	2.76	1.24	55.9	1.27
6H-4, 38-40	50.06	31.5	1.84	2.74	1.26	55.2	1.23
6H-5, 123-125	52.41	31.3	1.83	2.77	1.26	55.2	1.23
6H-6, 45-47	53.13	31.1	1.83	2.70	1.26	54.3	1.19
6H-7, 104-106	55.22	30.5	1.85	2.74	1.29	54.0	1.17
7H-2, 90-92	56.19	32.2	1.80	2.69	1.22	55.6	1.25
7H-3, 99-101	57.66	31.6	1.83	2.74	1.25	55.3	1.24
7H-4, 31-33	58.13	31.6	1.83	2.73	1.25	55.2	1.23
7H-6, 44-46	59.32	31.3	1.84	2.76	1.26	55.1	1.23
7H-7, 64-66	61.02	30.6	1.83	2.70	1.27	53.8	1.17
7H-8, 37-39	62.25	30.4	1.85	2.77	1.28	54.2	1.18
8H-2, 104-106	66.02	29.7	1.86	2.72	1.30	52.9	1.12
8H-3, 114-116	67.62	28.8	1.90	2.73	1.35	51.9	1.08
8H-4, 21-23	68.03	29.3	1.88	2.73	1.33	52.4	1.10
8H-5, 121-123	70.53	29.2	1.89	2.76	1.34	52.6	1.11
8H-6, 9-11	70.91	29.1	1.87	2.70	1.32	52.0	1.09
8H-7, 11-13	72.43	28.2	1.92	2.78	1.38	51.6	1.06
9H-1, 81-83	74.81	28.5	1.89	2.70	1.35	51.2	1.05
9H-2, 118-120	76.68	30.5	1.87	2.77	1.30	54.3	1.19
9H-3, 92-94	77.92	29.6	1.87	2.75	1.32	53.0	1.13
9H-4, 100-102	79.50	29.9	1.87	2.74	1.31	53.3	1.14
9H-5, 62-64	80.62	28.6	1.92	2.79	1.37	52.2	1.09
9H-6, 16-18	81.66	28.4	1.91	2.68	1.36	51.0	1.04
9H-7, 24-26	83.24	28.3	1.90	2.73	1.36	51.3	1.05
10X-1, 83-85	84.33	30.2	1.88	2.77	1.31	53.9	1.17
10X-2, 79-81	85.79	28.6	1.92	2.81	1.37	52.4	1.10
10X-3, 121-123	87.71	31.6	1.86	2.77	1.27	55.5	1.25
11X-2, 62-64	93.90	28.3	1.89	2.70	1.36	50.9	1.04
11X-3, 61-63	95.39	23.7	1.78	2.71	1.36	45.2	0.83
11X-4, 69-71	96.97	29.1	1.90	2.75	1.35	52.4	1.10
11X-5, 100-102	98.78	32.1	1.82	2.72	1.24	55.6	1.25
11X-6, 83-85	100.11	29.2	1.87	2.68	1.32	51.9	1.08
11X-7, 128-130	102.06	28.9	1.89	2.73	1.34	52.0	1.08
12X-1, 93-95	103.63	29.5	1.87	2.72	1.32	52.6	1.11
12X-2, 91-93	105.11	27.8	1.93	2.73	1.39	50.7	1.03
12X-3, 120-122	106.90	28.7	1.89	2.75	1.35	51.9	1.08
12X-4, 86-88	108.06	29.2	1.91	2.77	1.35	52.7	1.11
12X-5, 81-83	109.51	29.9	1.88	2.78	1.32	53.6	1.16
12X-6, 30-32	110.50	29.0	1.90	2.74	1.35	52.2	1.09
13X-1, 89-91	113.29	28.8	1.92	2.78	1.36	52.3	1.10
13X-2, 89-91	114.79	29.6	1.91	2.75	1.34	52.9	1.13
13X-3, 81-83	116.21	28.7	1.91	2.78	1.36	52.2	1.09
13X-4, 71-73	117.61	26.8	1.92	2.71	1.41	49.2	0.97
13X-5, 39-41	118.79	29.3	1.90	2.87	1.35	53.7	1.16
13X-6, 26-28	120.16	28.6	1.89	2.71	1.35	51.5	1.06
14X-1, 93-95	123.03	30.0	1.88	2.77	1.32	53.6	1.16
14X-2, 102-104	124.62	27.9	1.92	2.80	1.38	51.4	1.06
14X-3, 76-78	125.86	27.2	1.93	2.72	1.41	49.9	0.99
14X-4, 69-71	127.29	27.4	1.95	2.78	1.42	50.6	1.02
14X-5, 87-89	128.97	27.8	1.93	2.77	1.39	51.0	1.04
14X-6, 90-92	130.50	26.8	1.94	2.76	1.42	49.7	0.99
15X-1, 66-68	132.46	27.7	1.93	2.76	1.40	50.8	1.03
15X-2, 77-79	134.07	25.2	1.98	2.80	1.48	48.0	0.92

Table 11 (continued).

Core, section, interval (cm)	Depth (mbsf)	Water content (%)	Wet-bulk density (g/cm ³)	Grain density (g/cm ³)	Dry-bulk density (g/cm ³)	Porosity (%)	Void ratio
15X-3, 80-82	135.60	27.8	1.94	2.77	1.40	51.0	1.04
15X-4, 69-71	136.99	26.0	1.96	2.72	1.45	48.3	0.93
15X-5, 42-44	138.22	25.8	1.97	2.76	1.46	48.4	0.94
16X-1, 99-101	142.49	26.6	1.97	2.77	1.44	49.4	0.98
16X-2, 99-101	143.99	26.0	1.96	2.65	1.45	47.7	0.91
16X-3, 99-101	145.49	25.1	1.98	2.73	1.48	47.2	0.90
17X-1, 116-118	152.36	25.7	1.96	2.76	1.46	48.2	0.93
17X-2, 116-118	153.86	26.7	1.96	2.75	1.44	49.4	0.98
17X-3, 116-118	155.36	25.1	1.96	2.78	1.47	47.6	0.91
17X-4, 116-118	156.86	24.8	1.98	2.70	1.49	46.5	0.87
17X-5, 85-87	158.05	26.5	1.95	2.70	1.43	48.7	0.95
17X-6, 72-74	159.42	25.4	1.98	2.76	1.48	47.8	0.92
18X-1, 106-108	161.96	28.6	1.89	2.79	1.35	52.1	1.09
18X-2, 130-132	163.70	25.6	1.96	2.71	1.46	47.7	0.91
19X-1, 128-130	171.88	26.6	1.95	2.73	1.43	49.2	0.97
19X-2, 102-104	173.12	27.4	1.93	2.77	1.40	50.5	1.02
19X-3, 132-134	174.92	26.6	1.95	2.71	1.43	49.0	0.96
19X-4, 97-99	176.07	25.6	1.97	2.68	1.46	47.4	0.90
19X-5, 49-51	177.09	25.4	1.95	2.67	1.46	47.0	0.89
19X-6, 112-114	179.22		2.04				
19X-7, 44-46	180.04	24.7	2.01	2.69	1.51	46.3	0.86

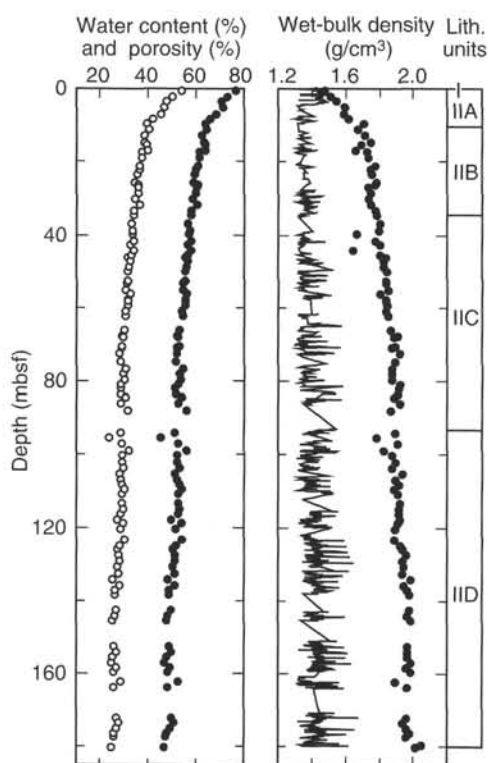


Figure 22. Water content (open circles) and porosity (solid circles), and wet-bulk density determined by discrete-sample measurements (circles) and the GRAPE (line) in Hole 937B.

suggesting that the clast was derived from a shallow-water interglacial sediment.

REFERENCES*

- Damuth, J.E., 1977. Late Quaternary sedimentation in the western equatorial Atlantic. *Geol. Soc. Am. Bull.*, 88:695-710.
- Damuth, J.E., Flood, R.D., Kowsmann, R.O., Belderson, R.H., and Gorini, M.A., 1988. Anatomy and growth pattern of Amazon deep-sea fan as revealed by long-range side-scan sonar (GLORIA) and high-resolution seismic studies. *AAPG Bull.*, 72:885-911.
- Manley, P.L., and Flood, R.D., 1988. Cyclic sediment deposition within Amazon deep-sea fan. *AAPG Bull.*, 72:912-925.

*Abbreviations for names of organizations and publications in ODP reference lists follow the style given in *Chemical Abstracts Service Source Index* (published by American Chemical Society).

Ms 155IR-113

NOTE: For all sites drilled, core-description forms ("barrel sheets") and core photographs can be found in Section 4, beginning on page 703. Forms containing smear-slide data can be found in Section 5, beginning on page 1199. GRAPE, index property, magnetic susceptibility, and natural gamma data are presented on CD-ROM (back pocket).

Table 12. Undrained shear strength at Site 937.

Core, section, interval (cm)	Depth (mbsf)	Peak undrained shear strength (kPa)	Residual undrained shear strength (kPa)	Unconfined compressive strength* (kPa)	Core, section, interval (cm)	Depth (mbsf)	Peak undrained shear strength (kPa)	Residual undrained shear strength (kPa)	Unconfined compressive strength* (kPa)
155-937B-					15X-1, 67	132.47	34.5	22.1	78.4
1H-1, 53	0.53	6.9	5.1		15X-2, 78	134.08	49.9	29.9	112.7
1H-2, 53	2.03	4.7	3.5		15X-3, 81	135.61	44.2	29.8	117.6
1H-3, 54	3.54	13.1	8.7		15X-4, 70	137.00	58.1	35.3	147.0
1H-4, 40	4.90	6.6	5.4		15X-5, 43	138.23	68.4	36.0	98.0
1H-5, 76	6.76	5.7	4.3		16X-1, 100	142.50	36.5	21.8	83.3
2H-1, 61	8.11	7.7	5.8		16X-2, 105	144.05	58.1	29.8	127.4
2H-2, 61	9.61	19.7	12.1		16X-3, 100	145.50	58.6	31.6	142.1
2H-3, 56	11.06	7.1	5.2		17X-1, 117	152.37	47.3	30.9	186.2
2H-4, 70	12.70	8.0	5.9		17X-2, 117	153.87	52.5	32.7	117.6
2H-5, 101	14.51	8.2	6.0		17X-3, 117	155.37	69.4	41.0	147.0
2H-6, 33	15.33	10.6	7.7		17X-4, 117	156.87	73.6	40.6	171.5
2H-7, 31	16.81	10.1	7.5		17X-5, 86	158.06	78.7	42.5	196.0
3H-1, 25	17.25	14.6	10.0		17X-6, 73	159.43	82.8	40.5	196.0
3H-2, 43	18.93	11.5	8.4		18X-1, 107	161.97	15.9	12.9	24.5
3H-3, 117	21.17	10.2	6.0		18X-2, 130	163.70	69.4	39.1	137.2
3H-4, 58	22.08	13.7	9.2		19X-1, 129	171.89	43.2	27.8	112.7
3H-5, 31	23.31	12.8	8.4		19X-2, 103	173.13	43.2	26.5	107.8
3H-6, 105	25.55	15.3	9.7		19X-3, 133	174.93	47.8	31.0	137.2
3H-7, 27	26.27	14.3	9.5		19X-4, 98	176.08	56.1	39.7	127.4
4H-1, 40	26.90	8.3	7.0		19X-5, 50	177.10	64.8	36.0	196.0
4H-2, 54	28.54	17.3	12.0		19X-6, 113	179.23	79.7	40.2	122.5
4H-3, 47	29.97	20.5	13.2		19X-7, 45	180.05	64.3	31.3	176.4
4H-4, 52	31.52	27.3	16.1						
4H-5, 61	33.11	27.9	16.0						
4H-6, 53	34.53	21.6	12.4						
5H-1, 71	36.71	19.5	12.6	19.6					
5H-2, 118	38.68	17.8	12.2	29.4					
5H-3, 65	39.65	19.4	13.2	39.2					
5H-4, 96	41.46	20.9	13.5	39.2					
5H-5, 71	42.71	20.0	13.5	49.0					
5H-6, 59	44.09	20.8	13.4	39.2					
5H-7, 58	45.58	20.9	15.0	49.0					
6H-1, 45	45.95	26.6	15.3	49.0					
6H-2, 38	47.06	24.3	16.1	49.0					
6H-3, 50	48.68	28.3	18.1	58.8					
6H-4, 38	50.06	24.6	15.2	58.8					
6H-5, 124	52.42	25.5	15.1	68.6					
6H-6, 46	53.14	24.6	16.6	49.0					
6H-7, 105	55.23	25.2	16.9	49.0					
7H-2, 92	56.21	19.2	14.0	49.0					
7H-3, 101	57.68	25.2	16.5	58.8					
7H-4, 31	58.13	19.2	14.0	29.4					
7H-6, 45	59.82			68.6					
7H-7, 64	61.02			68.6					
7H-8, 41	62.26	28.0	17.9	73.5					
8H-2, 104	66.02	31.1	17.0	73.5					
8H-3, 114	67.62	32.5	19.4	68.6					
8H-4, 21	68.03	19.2	12.0	68.6					
8H-5, 30	69.62	33.4	21.5	78.4					
8H-6, 10	70.92	32.9	22.0	78.4					
8H-7, 10	72.42	34.5	18.6	88.2					
9H-1, 85	74.85			88.2					
9H-2, 119	76.69	22.1	12.7	73.5					
9H-3, 92	77.92	43.7	25.3	88.2					
9H-4, 100	79.50	44.7	25.8	98.0					
9H-5, 63	80.63	42.7	24.4	98.0					
9H-6, 17	81.67	38.1	24.1	88.2					
9H-7, 24	83.24	48.9	30.5	102.9					
10X-1, 84	84.34	18.5	13.6	49.0					
10X-2, 80	85.80	21.1	15.2	68.6					
11X-2, 63	93.91	41.1	27.4	88.2					
11X-3, 61	95.39	39.1	25.1	98.0					
11X-4, 70	96.98	36.0	24.6	88.2					
11X-5, 100	98.78	21.6	15.9	68.6					
11X-6, 85	100.13	40.6	24.7	98.0					
11X-7, 128	102.06	42.7	27.7	107.8					
12X-1, 97	103.67			98.0					
12X-2, 92	105.12	31.9	22.6	88.2					
12X-3, 121	106.91	29.8	21.7	78.4					
12X-4, 87	108.07	34.5	23.7	88.2					
12X-5, 82	109.52	23.7	16.9	49.0					
12X-6, 31	110.51	42.2	25.3	53.9					
13X-1, 90	113.30	31.9	19.9	73.5					
13X-2, 90	114.80	38.6	21.3	63.7					
13X-3, 82	116.22	44.2	24.5	102.9					
13X-4, 72	117.62	51.9	26.3	93.1					
13X-5, 40	118.80	30.3	18.9	58.8					
13X-6, 27	120.17	43.2	28.3	98.0					
14X-1, 94	123.04	26.7	17.4	68.6					
14X-2, 103	124.63	39.1	21.3	98.0					
14X-3, 77	125.87	54.0	33.1	107.8					
14X-4, 70	127.30	66.9	38.1	142.1					
14X-5, 88	128.98	73.6	37.7	127.4					
14X-6, 91	130.51	76.1	41.6	156.8					

Note: * = unconfined compressive strength (q_u) can be used to approximate undrained shear strength (S_u) by the relationship $q_u = 2S_u$.

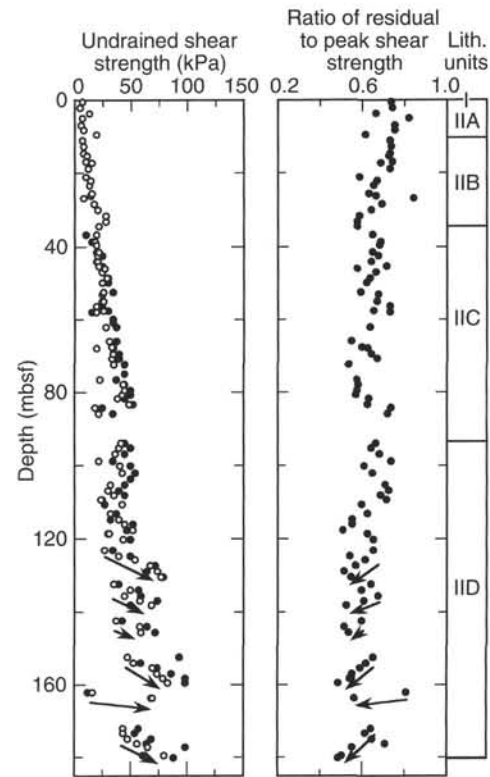


Figure 23. Left: Undrained shear strength (open circles) and assumed undrained shear strength derived from unconfined compressive strength (solid circles) in Hole 937B. Arrows indicate the trends of increasing shear strength with depth in Cores 937B-14X through -19X. Right: Ratio of residual to peak undrained shear strength. Arrows indicate the trends of decreasing residual/peak strength ratio with depth in Cores 937B-14X through -19X.

Table 13. Electrical resistivity at Site 937.

Core, section, interval (cm)	Depth (mbsf)	Longitudinal resistivity (Ωm)	Transverse resistivity (Ωm)	Core, section, interval (cm)	Depth (mbsf)	Longitudinal resistivity (Ωm)	Transverse resistivity (Ωm)
155-937B-				15X-3, 81	135.61	0.364	0.373
1H-1, 53	0.53	0.256	0.232	15X-4, 70	137.00	0.385	0.371
1H-2, 53	2.03	0.232	0.227	15X-5, 43	138.23	0.398	0.382
1H-3, 54	3.54	0.249	0.240	16X-1, 100	142.50	0.367	0.366
1H-4, 40	4.90	0.249	0.246	16X-2, 100	144.00	0.391	0.371
1H-5, 76	6.76	0.253	0.259	16X-3, 100	145.50	0.399	0.412
2H-1, 61	8.11	0.278	0.278	17X-1, 117	152.37	0.389	0.370
2H-2, 61	9.61	0.270	0.245	17X-2, 117	153.87	0.388	0.367
2H-3, 56	11.06	0.219	0.254	17X-3, 117	155.37	0.438	0.443
2H-4, 70	12.70	0.247	0.251	17X-4, 117	156.87	0.413	0.397
2H-5, 101	14.51	0.300	0.307	17X-5, 86	158.06	0.397	0.392
2H-6, 33	15.33	0.247	0.273	17X-6, 73	159.43	0.398	0.379
2H-7, 31	16.81	0.253	0.260	18X-1, 107	161.97	0.382	0.327
3H-1, 25	17.25	0.288	0.274	18X-2, 130	163.70	0.397	0.374
3H-2, 43	18.93	0.290	0.280	19X-1, 129	171.89	0.418	0.447
3H-3, 117	21.17	0.314	0.310	19X-2, 103	173.13	0.369	0.399
3H-4, 58	22.08	0.315	0.299	19X-3, 133	174.93	0.370	0.406
3H-5, 31	23.31	0.308	0.303	19X-4, 98	176.08	0.394	0.398
3H-6, 105	25.55	0.321	0.301	19X-5, 50	177.10	0.376	0.381
3H-7, 27	26.27	0.320	0.298	19X-6, 113	179.23	0.435	0.419
4H-1, 40	26.90	0.313	0.315	19X-7, 45	180.05	0.440	0.388
4H-2, 54	28.54	0.334	0.331				
4H-3, 47	29.97	0.343	0.332				
4H-4, 52	31.52	0.327	0.329				
4H-5, 61	33.11	0.336	0.321				
4H-6, 53	34.53	0.346	0.333				
5H-1, 71	36.71	0.358	0.354				
5H-2, 118	38.68	0.357	0.351				
5H-3, 65	39.65	0.353	0.353				
5H-4, 96	41.46	0.336	0.340				
5H-5, 71	42.71	0.351	0.346				
5H-6, 59	44.09	0.338	0.350				
5H-7, 58	45.58	0.359	0.362				
6H-1, 45	45.95	0.356	0.356				
6H-2, 38	47.06	0.360	0.362				
6H-3, 50	48.68	0.365	0.361				
6H-4, 38	50.06	0.375	0.371				
6H-5, 124	52.42	0.380	0.370				
6H-6, 45	53.13	0.371	0.356				
6H-7, 104	55.22	0.376	0.388				
7H-2, 92	56.21	0.357	0.357				
7H-3, 100	57.67	0.358	0.344				
7H-4, 30	58.12	0.340	0.355				
7H-6, 45	59.33	0.367	0.345				
7H-7, 65	61.03	0.401	0.408				
7H-8, 39	62.27	0.407	0.398				
8H-2, 104	66.02	0.384	0.367				
8H-3, 114	67.62	0.401	0.397				
8H-4, 21	68.03	0.396	0.418				
8H-5, 122	70.54	0.414	0.404				
8H-6, 10	70.92	0.402	0.397				
8H-7, 10	72.42	0.403	0.401				
9H-1, 82	74.82	0.393	0.394				
9H-2, 119	76.69	0.387	0.419				
9H-3, 93	77.93	0.394	0.403				
9H-4, 100	79.50	0.392	0.407				
9H-5, 63	80.63	0.454	0.415				
9H-6, 17	81.67	0.421	0.412				
9H-7, 25	83.25	0.400	0.394				
10X-1, 84	84.34	0.335	0.352				
10X-2, 80	85.80	0.389	0.363				
10X-3, 122	87.72	0.367	0.387				
11X-2, 63	93.91	0.391	0.388				
11X-3, 61	95.39	0.394	0.383				
11X-4, 70	96.98	0.375	0.395				
11X-5, 100	98.78	0.362	0.373				
11X-6, 85	100.13	0.411	0.394				
11X-7, 128	102.06	0.378	0.414				
12X-1, 93	103.63	0.409	0.386				
12X-2, 91	105.11	0.389	0.370				
12X-3, 121	106.91	0.397	0.374				
12X-4, 87	108.07	0.371	0.400				
12X-5, 82	109.52	0.396	0.347				
12X-6, 31	110.51	0.341	0.316				
13X-1, 90	113.30	0.386	0.387				
13X-2, 90	114.80	0.357	0.351				
13X-3, 82	116.22	0.348	0.343				
13X-4, 72	117.62	0.378	0.356				
13X-5, 40	118.80	0.338	0.350				
13X-6, 27	120.17	0.367	0.386				
14X-1, 94	123.04	0.348	0.361				
14X-2, 103	124.63	0.367	0.352				
14X-3, 77	125.87	0.360	0.351				
14X-4, 70	127.30	0.359	0.358				
14X-5, 88	128.98	0.365	0.360				
14X-6, 91	130.51	0.370	0.367				
15X-1, 67	132.47	0.368	0.344				
15X-2, 78	134.08	0.377	0.390				

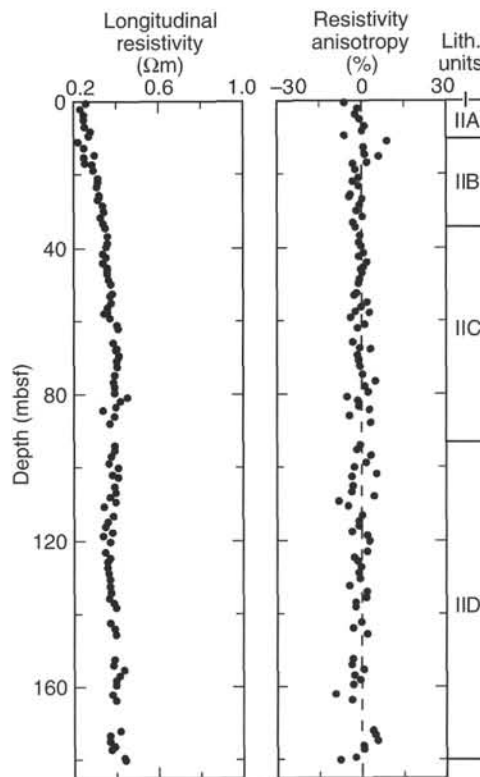


Figure 24. Longitudinal resistivity and resistivity anisotropy in Hole 937B.

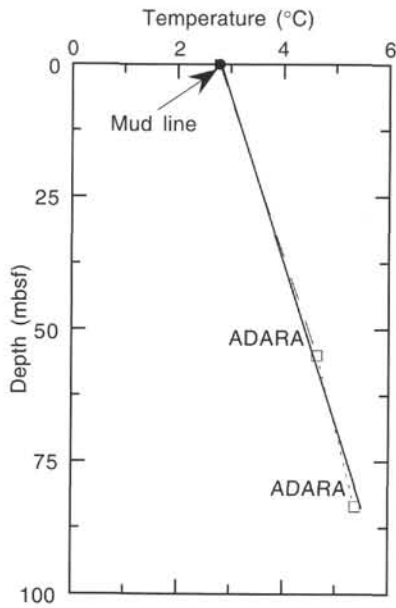


Figure 25. Estimated equilibrium temperatures in Hole 937B. A linear curve fit (solid line) through the data suggests that reliable equilibrium temperatures were acquired that indicate a geothermal gradient of 31.29°C/km. A geothermal temperature gradient of 33.8°C/km is calculated (dashed line) by using the ADARA mud-line temperature and the one ADARA measurement at 55.0 mbsf. A geothermal temperature gradient of 25.3°C/km is calculated (dotted line) by using both ADARA measurements.

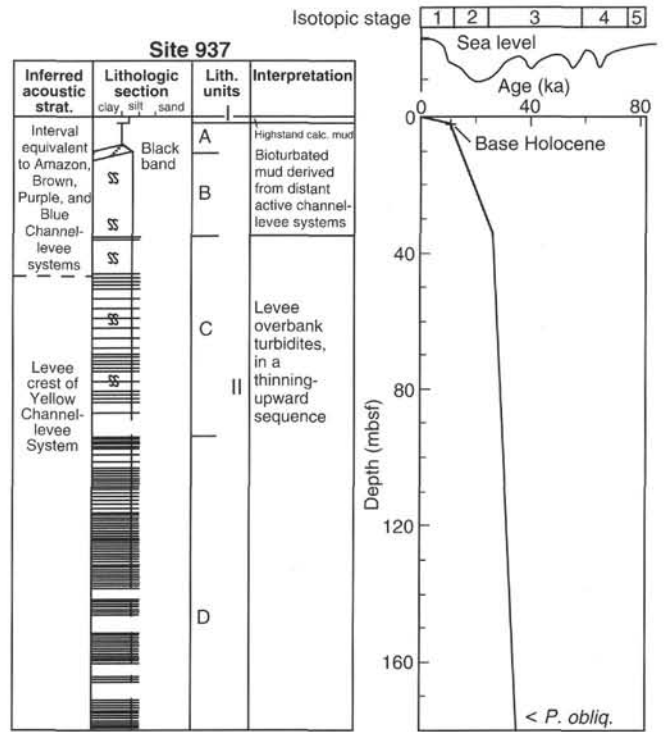


Figure 26. Summary of Site 937 showing (left to right) inferred acoustic stratigraphy, schematic lithologic column, lithologic units, interpreted sediment facies, chronological picks, and interpreted age-depth curve (+ = datums; < = younger than a datum; variations in slope between these points are interpreted, based on dated intervals of similar facies at other sites).